symmetry

MDPI

Article

A Caputo Fractional Tumour–Immune–Vaccine Model: Stability, Sensitivity and Semi-Analytical Solutions

Mustafa Ahmed Ali [1,2], Mehmet Merdan [2,*] and Mohamed Abubakar Fiidow [1]

[1] Department of Mathematics, Faculty of Science, Somali National University, Mogadishu P.O. Box 15, Somalia
[2] Department of Mathematical Engineering, Gümüşhane University, 29100 Gümüşhane, Turkey
* Correspondence: mmerdan@gumushane.edu.tr

Abstract

This study extends a tumour–immune–vaccine model to a Caputo fractional-order framework to describe memory effects in tumour growth, immune response, and vaccine clearance. The solutions are shown to remain non-negative, with the tumour burden bounded by the carrying capacity. The effector population is uniformly bounded when its death rate exceeds its proliferation rate $\eta > \rho$, and bounded only on finite time intervals otherwise. The vaccine concentration is obtained in closed form. A tumour invasion number $\mathcal{R}_T$ and an effector self-renewal number $\mathcal{R}_I$ are derived, and the tumour-free and coexistence equilibria are shown to be locally asymptotically stable under conditions on these thresholds that do not depend on the fractional order. With parameter values chosen from published ranges, the model predicts a stable coexistence state with a small residual tumour burden. Sensitivity analysis shows that the immune effector rates control the long-term tumour burden, whereas the tumour growth rate and carrying capacity dominate the early response. Approximate analytical solutions are obtained by the Yang transform Adomian decomposition method and validated against Runge–Kutta solutions for $q = 1$ and the fractional Adams–Bashforth–Moulton method for $0 < q < 1$. The results show that memory accelerates the initial response but slows the later growth of the tumour.

Keywords: Caputo fractional derivative; tumour–immune–vaccine model; Yang transform, Adomian decomposition method; tumour invasion number; stability analysis; sensitivity analysis

1. Introduction

Tumour progression depends on the balance between cancer cell proliferation and immune-mediated elimination, a balance that therapeutic interventions can shift. Cancer cells that escape immune surveillance continue to grow, whereas an effective immune response, supported by treatment, can suppress tumour growth. Mathematical models provide a quantitative framework for studying these interactions, identifying the conditions under which a tumour persists or regresses, and assessing how individual biological processes influence treatment outcomes. Early studies demonstrated that nonlinear interactions play a central role in tumour–immune dynamics. Kuznetsov et al. [1] analysed the dynamics of immunogenic tumours through parameter estimation and bifurcation analysis, and Kirschner and Panetta [2] developed a tumour–immune model incorporating immunotherapy. De Pillis and collaborators subsequently modelled the immune response to tumour invasion, cell-mediated tumour destruction, and combined immunotherapy and chemotherapy [3–5]. Eftimie et al. [6] later reviewed non-spatial tumour–immune models

Check for updates

Academic Editor: Mariano Torrisi

Received: 3 November 2026
Revised: 18 November 2026
Accepted: 21 November 2026
Published: 26 November 2026

Copyright: © 2026 by the authors. Licensee MDPI, Basel, Switzerland. This article is an open access article distributed under the terms and conditions of the Creative Commons Attribution (CC BY) license.

and the biological mechanisms represented by different formulations. Together, these studies laid the groundwork for models that explicitly incorporate therapeutic interventions such as vaccination.

Therapeutic vaccination adds a treatment component to tumour–immune dynamics, which requires models that account for vaccine administration and its biological effects. Castiglione and Piccoli studied cancer immunotherapy and optimal control, including dendritic cell transfection and vaccine scheduling [7–9]. De Pillis et al. [10] also developed a model of dendritic cell therapy for melanoma. Such formulations examine treatment exposure alongside tumour growth and immune activation. More recently, Kamran et al. [11] proposed a tumour–immune–vaccine model and compared its predicted tumour dynamics with clinical MRI measurements. However, their model is of integer order, whereas immune activation and vaccine-induced responses depend on past exposure, a memory effect that integer-order models cannot represent.

Fractional calculus and delay differential equations provide complementary frameworks for describing memory and temporal effects in physical and biological systems [12–16]. Their foundations include Caputo's work on dissipation [17], systematic treatments of fractional differential equations [18,19], a generalized Taylor formula [20], existence theory [21] and Lyapunov methods [22,23].

Fractional tumour–immune modelling has developed along several complementary directions. Öztürk and Özköse [24] examined stability in a fractional tumour–immune model, while Rihan and Velmurugan [25] investigated a fractional-order model with delay. Rihan and Udhayakumar subsequently considered vaccine efficacy within a fractional delay framework, addressing stability, bifurcation, and control [26]. Other contributions examined tumour dynamics using various operators, including Caputo, conformable, Caputo–Fabrizio, and fractional-fractal derivatives [27–29]. Data-oriented modelling of lung cancer and studies of chaotic tumour–effector dynamics further illustrate the questions addressed by fractional approaches [30,31].

Several other transform and series methods have been applied to fractional equations, including Aboodh-based methods [32–35], natural, Laplace-like, Sumudu and Laplace–ARA transforms [36–40], and residual power series, homotopy perturbation and variational iteration methods [41–44]. Among these, the Yang transform converts the Caputo derivative into an algebraic expression, and its combination with Adomian decomposition treats nonlinear terms systematically.

The development of integral-transform techniques has expanded analytical approaches for fractional-order differential equations. Yang introduced transform methods for steady heat-transfer [45], laying the foundation for subsequent applications. Ganie et al. [46,47] investigated fractional partial differential equations and the time-fractional nonlinear dispersive $K(m, n, 1)$ equations using the homotopy perturbation transform method and the Yang transform decomposition method. Abdali [48] explored an iterative YJ–Adomian decomposition approach for fractional differential equations, while Al-Griffi and Al-Saif [49] combined the Yang transform with homotopy perturbation to study non-Newtonian viscoelastic flow over a turbine disk. Naeem et al. [50] employed the Yang transform in a comparative study of fractional partial differential equations. Ganie et al. [51] examined a time-fractional coupled shallow-water system involving the Caputo derivative. More recently, Ali and Merdan [52,53] applied the Yang transform Adomian decomposition method to time-fractional coupled Burgers equations and the Swift–Hohenberg equation. These contributions motivate applying the Yang transform Adomian decomposition method to the fractional-order tumour–immune–vaccine system considered in this study.

Extending the model of [11] to fractional order involves several difficulties, including the nonlocal Caputo derivative, the slow algebraic decay of Mittag–Leffler functions, the loss of boundedness when $\eta \leq \rho$, and the accuracy of truncated series for $0 < q < 1$.

The main contribution of this study is the extension of an integer-order tumour–immune–vaccine model to a Caputo fractional-order framework, together with a combined qualitative and semi-analytical analysis of the resulting system, which has not been carried out for this model before. We establish non-negativity and uniform boundedness for $\eta > \rho$ and identify a positively invariant feasible region. Two threshold quantities are introduced, namely the tumour invasion number $\mathcal{R}_T = \alpha e/(\gamma\mu)$, derived using the next-generation matrix approach, and the effector self-renewal number $\mathcal{R}_I = \rho/\eta$. We derive conditions for the local asymptotic stability of the tumour-free and coexistence equilibria that are valid for every fractional order q, so that memory affects the transient behaviour but not the equilibria or their local stability. The degenerate case $\mathcal{R}_I = 1$ and the absence of chaotic behaviour are also discussed. Sensitivity analyses examine these thresholds, the residual tumour burden at the coexistence equilibrium, and the tumour burden during the early therapeutic window for several fractional orders. For the parameter values considered, the immune effector rates predominantly influence the residual tumour burden, whereas the tumour growth rate and carrying capacity dominate the early response. In addition, the Yang transform Adomian decomposition method is applied to construct explicit approximate series solutions, which are validated against Runge–Kutta solutions for $q = 1$ and the fractional Adams–Bashforth–Moulton method for $0 < q < 1$. The numerical results illustrate how fractional memory alters transient behaviour, producing a faster initial response and slower subsequent tumour evolution in the cases examined.

The remainder of this work is organized as follows. Section 2 presents the model, and Section 3 introduces the mathematical preliminaries. Section 4 establishes the feasible region and fundamental properties of the model. Section 5 examines the equilibria, tumour invasion number, stability, and sensitivity. Section 6 describes the Yang transform Adomian decomposition method, while Section 7 presents numerical applications. Finally, conclusions are presented in Section 8.

2. Model Formulation

The present study extends the integer-order tumour–immune–vaccine model of Kamran et al. [11] to a Caputo fractional-order framework. Let $T(t)$ denote the tumour burden in mL, $I(t)$ the activated immune effector cell population in millions of cells, and $V(t)$ the circulating vaccine concentration in mg/mL, where $t \geq 0$ denotes time in days. The evolution of tumour burden is determined by the balance between proliferation and removal. Proliferation is described by the logistic term $\alpha T(1 - T/K)$, where α is the intrinsic growth rate and K is the carrying capacity. Tumour removal is represented by $\beta IT + \gamma VT$, where β measures immune-mediated killing and γ describes the direct vaccine-associated effect assumed in the original model. These bilinear terms express interactions according to the mass-action principle. The effector cell population increases through vaccine–tumour interactions at rate δVT and cell proliferation at rate ρI, while natural cell death reduces the population at rate ηI. Thus, δ denotes the immune activation coefficient, ρ and η are the per-capita proliferation and death rates, and $\rho - \eta$ is the net per-capita growth rate of effector cells. Since recruitment requires both vaccine and tumour antigen, it ceases whenever either is absent. Vaccine concentration is governed by a constant administration

rate μ and first-order clearance eV, where e is the clearance coefficient. The following system describes the tumour–immune–vaccine model

$$\begin{cases} \dfrac{dT}{dt} = \alpha T\left(1 - \dfrac{T}{K}\right) - \beta IT - \gamma VT, \\ \dfrac{dI}{dt} = \delta VT + (\rho - \eta)I, \\ \dfrac{dV}{dt} = \mu - eV, \end{cases} \tag{1}$$

subject to

$$T(0) = T_0 \geq 0, \quad I(0) = I_0 \geq 0, \quad V(0) = V_0 \geq 0. \tag{2}$$

The dependence of T, I, and V on time is omitted where no ambiguity arises.

To investigate the role of memory, we replace the ordinary derivatives in system (1) with Caputo derivatives of a common order $q \in (0, 1]$. This operator accounts for the history of the state variables through a power-law kernel and permits the direct use of the initial conditions in (2). The fractional system takes the form

$$\begin{cases} {}^{C}D_t^q T(t) = \alpha T\left(1 - \dfrac{T}{K}\right) - \beta IT - \gamma VT, \\ {}^{C}D_t^q I(t) = \delta VT + (\rho - \eta)I, \\ {}^{C}D_t^q V(t) = \mu - eV, \end{cases} \tag{3}$$

where ${}^{C}D_t^q$ denotes the Caputo fractional derivative. For $q = 1$, system (3) reduces to the integer-order model (1). For $0 < q < 1$, it allows the influence of past states on the transient tumour, immune, and vaccine dynamics to be examined. Figure 1 summarizes the model interactions.

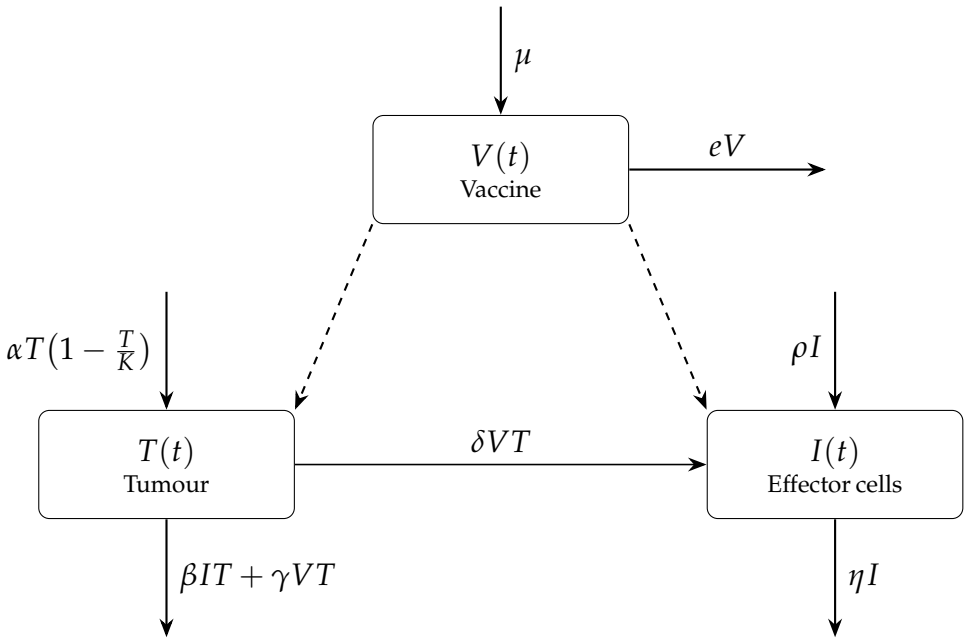


Figure 1. Compartmental flowchart of the tumour–immune–vaccine model. Dashed arrows indicate vaccine-associated tumour reduction ($V \to T$, $-\gamma VT$) and effector-cell recruitment ($V \to I$, $+\delta VT$).

Table 1 lists the parameter ranges and initial conditions reported by Kamran et al. [11]. Unless stated otherwise, all computations use the baseline set

$$\begin{aligned} &\alpha = 0.425, \quad K = 0.400, \quad \beta = 0.110, \quad \gamma = 0.0525, \quad \delta = 0.160, \\ &\rho = 0.050, \quad \eta = 0.080, \quad \mu = 1.250, \quad e = 0.600, \end{aligned} \tag{4}$$

in which each parameter is the midpoint of its range, except ρ, which is taken at the lower end of its range so that $\eta > \rho$ ($\mathcal{R}_I < 1$), the regime in which the effector population is uniformly bounded. The ranges in Table 1 also admit $\rho \geq \eta$. In that regime the solutions are bounded only on finite time intervals, and the effector population can grow without bound. These values provide a representative setting for numerical investigation; the fractional model is not independently fitted to clinical data in this study. Table 2 compares the present study with related tumour–immune models.

Table 1. Parameters and their values for the tumour–immune–vaccine model.

Notation	Description	Values	Units
α	Growth rate of tumour cells	(0.2–0.65)	cell^{-1}
β	Rate of tumour-killing by immune cells	(0.02–0.2)	cell^{-1}
γ	Rate of tumour-killing by vaccine	(0.005–0.1)	cell^{-1}
K	Carrying capacity of tumour cells	(0.25–0.55)	cell^{-1}
δ	Activation rate of immune cells due to tumour and vaccine	(0.02–0.3)	cell^{-1}
ρ	Proliferation rate of immune cells	(0.05–0.7)	day^{-1}
η	Natural death rate of immune cells	(0.01–0.15)	day^{-1}
μ	Amount of vaccine	(0.5–2.0)	cell^{-1}
e	Drug decay rate	(0.2–1.0)	$\text{cell}^{-1}\,\text{day}^{-1}$
T_0	Initial tumour volume	0.113	mL
I_0	Initial immune cell population	1.0	million cells
V_0	Initial vaccine concentration	1.5	mg/mL

Table 2. Comparison of the present study with related tumour–immune models.

Ref.	Derivative	Treatment	Main Focus
[11]	Integer order	Vaccine	Tumour–immune–vaccine model validated with clinical MRI data
[24]	Caputo	None	Stability analysis and fitting to experimental data
[25]	Fractional, delay	External treatment	Stability and Hopf bifurcation with respect to the delays
[26]	Fractional, delay	Vaccine efficacy	Stability, bifurcation and control
[27]	Caputo, conformable	None	Stability, and Neimark–Sacker bifurcation of a discretized model
[28]	Caputo, Caputo–Fabrizio	IL-12, anti-PD-L1	Stability, existence and uniqueness, reduction in cancer cells
[29]	Fractional, fractal–fractional	None	Tumour–healthy–effector dynamics with new operators
[30]	Caputo	None	Tumour–macrophage model of lung cancer with real data
[31]	Atangana–Baleanu	None	Chaotic dynamics, ABM and Toufik–Atangana schemes
Present	Caputo	Vaccine compartment	Thresholds $\mathcal{R}_T$ and $\mathcal{R}_I$, order-independent stability, boundedness, sensitivity, absence of chaos, YTADM series validated against ABM

3. Preliminary Concepts

This section recalls the definitions and basic properties of the Yang transform and the Caputo fractional derivative used in this study.

Definition 1 ([45]). *The Yang transform (YT) is defined as*

$$\mathrm{Y}[\Theta(t)] = \int_0^\infty e^{-\frac{t}{\chi}} \Theta(t) dt = \mathscr{R}(\chi), \ \chi > 0, \tag{5}$$

with inverse yang transform is given by: $\mathrm{Y}^{-1}[\mathscr{R}(\chi)] = \Theta(t)$.

Remark 1. *The following defines the Yang transformation of a few useful functions*

$$\mathsf{Y}[1] = \chi,\ \mathsf{Y}[t] = \chi^2,\ \mathsf{Y}[t^n] = \Gamma(n+1)\chi^{n+1},\ n \geq 0.$$

Definition 2 ([52,53]). *Let $\Theta(t)$ be sufficiently smooth with respect to t. The Caputo fractional derivative is defined as*

$${}^{C}D_t^q\Theta(t) = \begin{cases} \dfrac{1}{\Gamma(n-q)}\displaystyle\int_0^t (t-\sigma)^{n-q-1}\Theta^{(n)}(\sigma)d\sigma, & n-1 < q < n, \\ \dfrac{\partial^n}{\partial t^n}\Theta(t) & q = n \in \mathbb{N}. \end{cases} \tag{6}$$

Proposition 1 ([52,53]). *The Yang transform of the n^{th} derivative is defined as*

$$\mathsf{Y}\left[\Theta^{(n)}(t)\right] = \frac{\mathscr{R}(\chi)}{\chi^n} - \sum_{r=0}^{n-1}\frac{\Theta^{(r)}(0)}{\chi^{n-(r+1)}}. \tag{7}$$

Proposition 2 ([52,53]). *The Yang transform of the Caputo fractional derivative is defined*

$$\mathsf{Y}\left[{}^{C}D_t^q\Theta(t)\right] = \frac{\mathscr{R}(\chi)}{\chi^q} - \sum_{r=0}^{n-1}\frac{\Theta^{(r)}(0)}{\chi^{q-(r+1)}},\ n-1 < q \leq n,\ n \in \mathbb{N}. \tag{8}$$

Definition 3 ([54]). *The Mittag-Leffler functions are defined by the series*

$$E_q(z) = \sum_{k=0}^{\infty}\frac{z^k}{\Gamma(qk+1)}, \quad 0 < E_q(-bt^q) \leq 1 \quad \text{for } b > 0,\ t \geq 0,\ 0 < q \leq 1. \tag{9}$$

4. Some Fundamental Results About the Model

This section examines whether the fractional system (3) is biologically meaningful. Its solutions remain non-negative, and the tumour burden remains bounded by the carrying capacity. Uniform boundedness of the effect or population, and hence the existence of an attracting feasible region, holds under the condition $\eta > \rho$. For $\eta \leq \rho$, we obtain bounds valid only on finite time intervals.

Non-Negativity and Feasible Region

Lemma 1 (Non-negativity). *For any initial condition (2) with $T_0, I_0, V_0 \geq 0$, the solution of system (3) remains in $\mathbb{R}^3_+$ for all $t \geq 0$.*

Proof. On each boundary plane of $\mathbb{R}^3_+$, the vector field of system (3) points inward or is tangent

$${}^{C}D_t^q T\big|_{T=0} = 0, \quad {}^{C}D_t^q I\big|_{I=0} = \delta VT \geq 0, \quad {}^{C}D_t^q V\big|_{V=0} = \mu > 0. \tag{10}$$

By the invariance criterion for Caputo systems based on the generalized mean value theorem, the non-negative octant is positively invariant. □

Lemma 2 (Vaccine profile). *The solution of the third equation of system (3) is*

$$V(t) = \frac{\mu}{e} + \left(V_0 - \frac{\mu}{e}\right)E_q\left(-et^q\right), \tag{11}$$

so that V is monotone, $V(t) \to \mu/e$ as $t \to \infty$, and

$$V_{\min} := \min\left\{V_0, \frac{\mu}{e}\right\} \leq V(t) \leq \max\left\{V_0, \frac{\mu}{e}\right\} =: V_{\max}. \tag{12}$$

Proof. Applying the Yang transform to the third equation of (3) and using $V(0) = V_0$ gives

$$\frac{\mathcal{V}(\chi)}{\chi^q} - \frac{V_0}{\chi^{q-1}} = \mu\chi - e\mathcal{V}(\chi) \quad \Longrightarrow \quad \mathcal{V}(\chi) = \frac{\chi V_0 + \mu\chi^{q+1}}{1 + e\chi^q}. \tag{13}$$

Expanding $(1 + e\chi^q)^{-1} = \sum_{k\geq 0}(-e)^k\chi^{qk}$ and applying the inverse Yang transform with Remark 1, we obtain

$$V(t) = V_0 \sum_{k=0}^{\infty} \frac{(-e\,t^q)^k}{\Gamma(qk+1)} + \mu \sum_{m=1}^{\infty} \frac{(-e)^{m-1}t^{qm}}{\Gamma(qm+1)} = V_0 E_q(-e\,t^q) + \frac{\mu}{e}\left[1 - E_q(-et^q)\right], \tag{14}$$

which is (11). Since $V(t)$ is a convex combination of V_0 and μ/e with weights $E_q(-et^q) \in (0,1]$ and $1 - E_q(-et^q)$, the bounds (12) follow from Definition 3. □

Theorem 1 (Feasible region). *Let $T_0 \leq K$, and let $V_{\min}$ and $V_{\max}$ be given by (12), so that they depend on V_0. Then $T(t) \leq K$ for all $t \geq 0$. If, moreover, $\eta > \rho$, the effector population satisfies*

$$I(t) \leq \frac{B}{\eta - \rho} + \left(I_0 - \frac{B}{\eta - \rho}\right) E_q\big(-(\eta - \rho)t^q\big), \quad B = \delta V_{\max} K, \tag{15}$$

so that I is uniformly bounded, with $\sup_{t\geq 0} I(t) \leq \max\{I_0,\, B/(\eta - \rho)\}$ and $\limsup_{t\to\infty} I(t) \leq B/(\eta - \rho)$, and the compact set

$$\Psi = \left\{(T, I, V) \in \mathbb{R}^3_+ : T \leq K, \quad I \leq \frac{B}{\eta - \rho}, \quad V_{\min} \leq V \leq V_{\max}\right\} \tag{16}$$

has the following properties.

(a) Positive invariance: every solution with initial value in Ψ remains in Ψ for all $t \geq 0$.

(b) Asymptotic attraction. Every solution with $T_0 \leq K$ satisfies $\operatorname{dist}\big((T, I, V)(t), \Psi\big) \to 0$ as $t \to \infty$.

(c) Finite-time entry into a neighbourhood: for every $\varepsilon > 0$, every solution with $T_0 \leq K$ enters the set $\Psi_\varepsilon = \{(T, I, V) \in \mathbb{R}^3_+ : T \leq K,\ I \leq B/(\eta - \rho) + \varepsilon,\ V_{\min} \leq V \leq V_{\max}\}$ in finite time and remains in it afterward.

If $I_0 > B/(\eta - \rho)$, entry into Ψ itself in finite time is not guaranteed. If instead $\rho > \eta$, then

$$I(t) \leq \left(I_0 + \frac{B}{\rho - \eta}\right) E_q\big((\rho - \eta)t^q\big) - \frac{B}{\rho - \eta}, \tag{17}$$

and if $\rho = \eta$, then

$$I(t) \leq I_0 + \frac{Bt^q}{\Gamma(q+1)}. \tag{18}$$

In these two cases, the solution is bounded on every compact interval $[0, t_f]$, where $t_f > 0$ is an arbitrary finite final time, but the bounds (17) and (18) grow without limit as $t_f \to \infty$, so uniform boundedness is not established. For $\rho > \eta$ the effector population can indeed be unbounded. Hence uniform boundedness of system (3) is guaranteed only when $\eta > \rho$.

Proof. Fix $\varepsilon > 0$ and suppose that $t_1 > 0$ is the first time at which $T(t_1) = K + \varepsilon$, so that $T(t_1)$ is a maximum on $[0, t_1]$. For $0 < q < 1$, the Caputo extremum principle gives ${}^C D_t^q T(t_1) \geq 0$. For $q = 1$, the same conclusion follows from the first-contact property. However, by Lemma 1, evaluating the first equation of (3) at t_1 gives

$${}^C D_t^q T(t_1) = \alpha(K + \varepsilon)\left(1 - \frac{K + \varepsilon}{K}\right) - \left[\beta I(t_1) + \gamma V(t_1)\right](K + \varepsilon) < 0, \tag{19}$$

a contradiction. Hence $T(t) < K + \varepsilon$, and letting $\varepsilon \to 0$ yields $T(t) \le K$ for all $t \ge 0$.

Let now $\eta > \rho$. Using $T \le K$ and $V \le V_{\max}$ in the second equation of (3) gives

$$ {}^{C}D_t^q I(t) \le \delta V_{\max} K - (\eta - \rho) I(t) = B - (\eta - \rho) I(t), \tag{20} $$

and the fractional comparison principle yields (15). Since $E_q(-(\eta-\rho)t^q)$ decreases to zero, the right-hand side of (15) tends to $B/(\eta-\rho)$. In particular, if $I_0 \le B/(\eta-\rho)$, then $I(t) \le B/(\eta-\rho)$ for all $t \ge 0$. Together with the tumour bound and Lemma 2, this proves that Ψ is positively invariant, which is property (a). If $I_0 > B/(\eta-\rho)$, then

$$ \max\Big\{ I(t) - \frac{B}{\eta-\rho}, 0 \Big\} \le \Big(I_0 - \frac{B}{\eta-\rho} \Big) E_q\big(-(\eta-\rho)t^q\big) \longrightarrow 0, \tag{21} $$

which proves the attraction property (b). Since $E_q(-(\eta-\rho)t^q) > 0$ for all $t \ge 0$, inequality (21) does not guarantee that $I(t) \le B/(\eta-\rho)$ at any finite time. However, for $0 < q \le 1$ the function $t \mapsto E_q(-(\eta-\rho)t^q)$ is continuous and strictly decreasing from 1 to 0 [55]. Hence, for every $\varepsilon > 0$, there is a unique $t_\varepsilon > 0$ such that

$$ \Big(I_0 - \frac{B}{\eta-\rho} \Big) E_q\big(-(\eta-\rho)t_\varepsilon^q \big) = \varepsilon, $$

and by (21), $I(t) \le B/(\eta-\rho) + \varepsilon$ for all $t \ge t_\varepsilon$. Thus the solution enters Ψ_ε no later than t_ε and remains in it, which proves (c).

Finally, if $\rho > \eta$, the same bounds give ${}^{C}D_t^q I \le B + (\rho-\eta)I$, and comparison with the solution of ${}^{C}D_t^q y = B + (\rho-\eta)y$, $y(0) = I_0$, yields (17). If $\rho = \eta$, applying the fractional integral of order q to ${}^{C}D_t^q I \le B$ yields (18). □

For the baseline values (4) with the initial vaccine level $V_0 = 1.5$ of Table 1, we have $\eta > \rho$, $V_{\min} = V_0 = 1.5$, $V_{\max} = \mu/e = 2.0833$ and $B = 0.1333$, so that

$$ \Psi = \{ T \le 0.400,\ I \le 4.4444,\ 1.5 \le V \le 2.0833 \}. $$

The baseline initial state $(T_0, I_0, V_0) = (0.113, 1.0, 1.5)$ lies in Ψ, so by property (a) the corresponding solution remains in Ψ for all $t \ge 0$. These numerical bounds hold only for $V_0 = 1.5$. For other non-negative initial conditions (2), $V_{\min}$, $V_{\max}$ and B must be recomputed from (12). If, moreover, $I_0 > B/(\eta-\rho)$, the solution approaches Ψ asymptotically and enters Ψ_ε in finite time for every $\varepsilon > 0$.

5. Equilibrium Points and the Tumour Invasion Number

Equilibria are obtained by setting the right-hand sides of Equation (3) equal to zero, which gives

$$ (\eta - \rho) I^* = \delta V^* T^*. \tag{22} $$

The first equation factorizes as $T^*\left[\alpha(1 - T^*/K) - \beta I^* - \gamma V^*\right] = 0$, giving two cases.

5.1. Tumour-Free Equilibrium

For $T^* = 0$ and $\eta \ne \rho$ (that is, $\mathcal{R}_I \ne 1$), relation (22) forces $I^* = 0$, so

$$ \mathcal{E}^0 = \Big(0,\ 0,\ \frac{\mu}{e} \Big), \tag{23} $$

which exists for all admissible parameter values and represents complete remission under a maintained vaccine level.

The degenerate case $\eta = \rho$ ($\mathcal{R}_I = 1$).

If $\eta = \rho$, relation (22) reduces to $\delta V^* T^* = 0$. Since $V^* = \mu/e > 0$, every equilibrium has $T^* = 0$, so no coexistence equilibrium exists. With $T^* = 0$, relation (22) holds for every $I^* \geq 0$. The tumour-free equilibria therefore form the half-line

$$\mathcal{L} = \left\{ \mathcal{E}_I = \left(0, I, \frac{\mu}{e}\right) : I \geq 0 \right\}, \tag{24}$$

and $\mathcal{E}^0 = \mathcal{E}_{I=0}$ is no longer an isolated equilibrium. Its stability is discussed in Section 5.4.2.

5.2. Coexistence Equilibrium

For $T^* > 0$ we substitute I^* from Equation (22) into $\alpha(1 - T^*/K) = \beta I^* + \gamma V^*$ and solve, obtaining

$$\mathcal{E}^* = (T^*, I^*, V^*), \quad T^* = \frac{\mathcal{N}}{\mathcal{D}}, \quad I^* = \frac{\delta \mu T^*}{e(\eta - \rho)}, \quad V^* = \frac{\mu}{e}, \tag{25}$$

with

$$\mathcal{N} = \alpha - \frac{\gamma \mu}{e}, \quad \mathcal{D} = \frac{\alpha}{K} + \frac{\beta \delta \mu}{e(\eta - \rho)}. \text{ where } \mathcal{D}_1 = \frac{\alpha}{K}, \text{ and } \mathcal{D}_2 = \frac{\beta \delta \mu}{e(\eta - \rho)} \tag{26}$$

Since $\mathcal{D} > 0$ when $\eta > \rho$, positivity of T^* additionally requires $\mathcal{N} > 0$. The expressions (25) and (26) require $\eta \neq \rho$. For $\eta = \rho$, no coexistence equilibrium exists.

5.3. Tumour Invasion Number

Following the next-generation matrix technique [56], we treat the tumour as the single invading compartment, the effector and vaccine classes playing the role of the environment. Writing the tumour equation as a gain minus a loss,

$$\mathcal{F} = \left[\alpha T\right], \quad \mathcal{G} = \left[\frac{\alpha}{K} T^2 + \beta I T + \gamma V T\right], \tag{27}$$

and linearizing at $\mathcal{E}^0$, gives

$$F = \left[\alpha\right], \quad G = \left[\frac{\gamma \mu}{e}\right], \quad FG^{-1} = \left[\frac{\alpha e}{\gamma \mu}\right]. \tag{28}$$

The spectral radius of FG^{-1} defines the tumour invasion number

$$\mathcal{R}_T = \frac{\alpha e}{\gamma \mu} = \frac{\alpha}{\gamma V^*} \tag{29}$$

which compares the intrinsic proliferation rate of the tumour with the killing rate exerted by the vaccine at its sustained circulating level $V^* = \mu/e$. Because the effector compartment carries the autonomous term $(\rho - \eta)I$, a second dimensionless quantity is needed to characterize the immune response,

$$\mathcal{R}_I = \frac{\rho}{\eta}, \tag{30}$$

the effector self-renewal number, which compares proliferation with natural death of the effector pool in the absence of antigenic stimulation. In terms of Equations (29) and (30),

$$\mathcal{N} = \frac{\gamma \mu}{e}(\mathcal{R}_T - 1), \quad \eta - \rho = \eta(1 - \mathcal{R}_I), \tag{31}$$

so $T^* > 0$ and $I^* > 0$ hold simultaneously if and only if

$$\mathcal{R}_T > 1 \quad \text{and} \quad \mathcal{R}_I < 1. \tag{32}$$

For the baseline values of Table 1,

$$\mathcal{R}_T = \frac{0.425 \times 0.600}{0.0525 \times 1.250} = 3.8857, \quad \mathcal{R}_I = \frac{0.050}{0.080} = 0.6250, \tag{33}$$

so condition (32) holds and, in addition to $\mathcal{E}^0$, the model admits the coexistence equilibrium $\mathcal{E}^*$ in $\mathbb{R}^3_+$ for the baseline parameter set.

5.4. Stability Analysis

For a Caputo fractional system of order $q \in (0, 1]$, the local asymptotic stability of an equilibrium is decided by the arguments of the eigenvalues λ_i of the Jacobian matrix evaluated at that point

$$|\arg(\lambda_i)| > \frac{q\pi}{2}, \quad i = 1, 2, \ldots, n. \tag{34}$$

For $q = 1$ this reduces to the classical condition $\mathrm{Re}(\lambda_i) < 0$. A real negative eigenvalue has $\arg\lambda = \pi > q\pi/2$ for every $q \in (0, 1]$ and therefore always satisfies Equation (34), while a real positive eigenvalue has $\arg\lambda = 0$ and always violates it.

The Jacobian matrix of system (3) at a point (T, I, V) is

$$J(T, I, V) = \begin{pmatrix} \alpha - \dfrac{2\alpha T}{K} - \beta I - \gamma V & -\beta T & -\gamma T \\ \delta V & \rho - \eta & \delta T \\ 0 & 0 & -e \end{pmatrix}. \tag{35}$$

5.4.1. Local Stability of the Tumour-Free Equilibrium

Theorem 2. *The tumour-free equilibrium $\mathcal{E}^0$ is locally asymptotically stable for every $q \in (0, 1]$ if $\mathcal{R}_T < 1$ and $\mathcal{R}_I < 1$, and unstable if $\mathcal{R}_T > 1$ or $\mathcal{R}_I > 1$. The stability type of $\mathcal{E}^0$ does not depend on the fractional order. If $\mathcal{R}_I = 1$, then $\mathcal{E}^0$ is not an isolated equilibrium and is not asymptotically stable.*

Proof. Setting $T = I = 0$ and $V = \mu/e$ in (35) gives the lower-triangular matrix

$$J(\mathcal{E}^0) = \begin{pmatrix} \alpha - \dfrac{\gamma\mu}{e} & 0 & 0 \\ \dfrac{\delta\mu}{e} & \rho - \eta & 0 \\ 0 & 0 & -e \end{pmatrix}, \tag{36}$$

whose characteristic equation factorizes completely,

$$\det\big(J(\mathcal{E}^0) - \lambda\mathbb{I}\big) = -\Big(\lambda - \alpha + \frac{\gamma\mu}{e}\Big)\big(\lambda - \rho + \eta\big)\big(\lambda + e\big) = 0. \tag{37}$$

Hence the eigenvalues are

$$\lambda_1 = \alpha - \frac{\gamma\mu}{e} = \frac{\gamma\mu}{e}\big(\mathcal{R}_T - 1\big), \quad \lambda_2 = \rho - \eta = \eta\big(\mathcal{R}_I - 1\big), \quad \lambda_3 = -e < 0. \tag{38}$$

All three are real, so $\arg\lambda_i \in \{0, \pi\}$ and, since $q\pi/2 \le \pi/2 < \pi$, condition (34) holds for λ_i when $\lambda_i < 0$ and fails when $\lambda_i > 0$, for every $q \in (0, 1]$. As $\lambda_3 < 0$ always, $\mathcal{E}^0$ is locally asymptotically stable if and only if $\lambda_1 < 0$ and $\lambda_2 < 0$, that is, $\mathcal{R}_T < 1$ and $\mathcal{R}_I < 1$, and it is unstable as soon as one of these thresholds exceeds unity. □

5.4.2. Stability in the Degenerate Case $\eta = \rho$

When $\eta = \rho$, setting $T = 0$, $I \geq 0$ and $V = \mu/e$ in (35) gives

$$J(\mathcal{E}_I) = \begin{pmatrix} \alpha - \beta I - \dfrac{\gamma\mu}{e} & 0 & 0 \\ \dfrac{\delta\mu}{e} & 0 & 0 \\ 0 & 0 & -e \end{pmatrix}, \tag{39}$$

with eigenvalues

$$\lambda_1 = \beta\,(I_c - I), \quad \lambda_2 = 0, \quad \lambda_3 = -e, \quad I_c = \frac{\alpha - \gamma\mu/e}{\beta} = \frac{\gamma\mu}{\beta e}\,(\mathcal{R}_T - 1). \tag{40}$$

Since $\lambda_2 = 0$, condition (34) fails, so no point of $\mathcal{L}$ is locally asymptotically stable for any $q \in (0, 1]$, and Theorem 2 does not apply. If $\mathcal{R}_T > 1$, the equilibria with $I > I_c$ are stable but not asymptotically stable, while those with $I < I_c$, including $\mathcal{E}^0$, are unstable. For $q = 1$, since $dI/dt = \delta VT \geq 0$, the tumour is cleared, $T(t) \to 0$, and $I(t)$ tends to a limit $I_\infty \geq I_c$ that depends on the initial data.

5.4.3. Local Stability of the Coexistence Equilibrium

Theorem 3. *Whenever the coexistence equilibrium $\mathcal{E}^*$ of Equation (25) is feasible, i.e., whenever $\mathcal{R}_T > 1$ and $\mathcal{R}_I < 1$, it is locally asymptotically stable for every fractional order $q \in (0, 1]$.*

Proof. At $\mathcal{E}^*$ the equilibrium relation

$$\alpha\left(1 - \frac{T^*}{K}\right) - \beta I^* - \gamma V^* = 0 \tag{41}$$

holds, so the first diagonal entry of Equation (35) simplifies to

$$\alpha - \frac{2\alpha T^*}{K} - \beta I^* - \gamma V^* = \left[\alpha - \frac{\alpha T^*}{K} - \beta I^* - \gamma V^*\right] - \frac{\alpha T^*}{K} = -\frac{\alpha T^*}{K}, \tag{42}$$

and the Jacobian becomes

$$J(\mathcal{E}^*) = \begin{pmatrix} -\dfrac{\alpha T^*}{K} & -\beta T^* & -\gamma T^* \\ \dfrac{\delta\mu}{e} & -(\eta - \rho) & \delta T^* \\ 0 & 0 & -e \end{pmatrix}. \tag{43}$$

Expanding along the last row, the characteristic equation factorizes as

$$(\lambda + e)\left(\lambda^2 + a_1\lambda + a_2\right) = 0, \tag{44}$$

where

$$a_1 = \frac{\alpha T^*}{K} + (\eta - \rho), \quad a_2 = \frac{\alpha T^*}{K}(\eta - \rho) + \frac{\beta\delta\mu T^*}{e}. \tag{45}$$

Thus $\lambda_3 = -e < 0$, and $\lambda_{1,2}$ solve the quadratic factor. Feasibility gives $T^* > 0$ and $\eta - \rho = \eta(1 - \mathcal{R}_I) > 0$, so

$$a_1 > 0, \quad a_2 > 0, \tag{46}$$

and by the Routh–Hurwitz criterion for a quadratic, both roots have negative real part. If the discriminant $\Delta = a_1^2 - 4a_2 \geq 0$ the roots are real and negative, so $|\arg \lambda_{1,2}| = \pi$. If $\Delta < 0$, then

$$\lambda_{1,2} = -\frac{a_1}{2} \pm \frac{i}{2}\sqrt{4a_2 - a_1^2}, \quad |\arg \lambda_{1,2}| = \pi - \arctan\left(\frac{\sqrt{4a_2 - a_1^2}}{a_1}\right) > \frac{\pi}{2}, \tag{47}$$

since the arctangent of a positive argument is smaller than $\pi/2$. In both cases $|\arg \lambda_i| > \pi/2 \geq q\pi/2$ for $i = 1,2,3$ and all $q \in (0,1]$, so condition (34) is satisfied and $\mathcal{E}^*$ is locally asymptotically stable. □

Figures 2 and 3 show the behaviour of the model for two choices of the vaccine parameters γ and e, with $\mathcal{R}_I = 0.625 < 1$ in both cases. All values lie within the ranges of Table 1. In Figure 2, the vaccine killing rate is raised to $\gamma = 0.10$ and the clearance rate is lowered to $e = 0.25$ day^{-1}, so that the invasion number is $\mathcal{R}_T = 0.8500 < 1$ and the eigenvalues (38) are $\lambda_1 = -0.075$, $\lambda_2 = -0.030$ and $\lambda_3 = -0.250$. By Theorem 2 the tumour-free equilibrium is stable, and the numerical solution converges to $\mathcal{E}^0 = (0, 0, 5.0000)$. Figure 3 corresponds to the baseline values, for which the invasion number is $\mathcal{R}_T = 3.8857 > 1$. $\mathcal{E}^0$ loses stability, the coexistence equilibrium becomes feasible, and the solution converges to

$$\mathcal{E}^* = \big(0.1381 \text{ mL},\ 1.5350 \text{ million cells},\ 2.0833 \text{ mg/mL}\big), \tag{48}$$

in agreement with the closed form (25) to all displayed digits. For this equilibrium $a_1 = 0.1768$, $a_2 = 0.0095$ and $\Delta = -0.0066 < 0$, so that

$$\lambda_{1,2} = -0.08839 \pm 0.04069\, i, \quad \lambda_3 = -0.600, \quad |\arg \lambda_{1,2}| = 0.8627\,\pi > \frac{q\pi}{2} \ \ \forall q \in (0,1], \tag{49}$$

confirming Theorem 3: $\mathcal{E}^*$ is a stable focus, which appears in Figure 3 as a transient overshoot of the tumour burden, reaching $T = 0.1721$ at $t \approx 11.8$ days before settling at T^*.

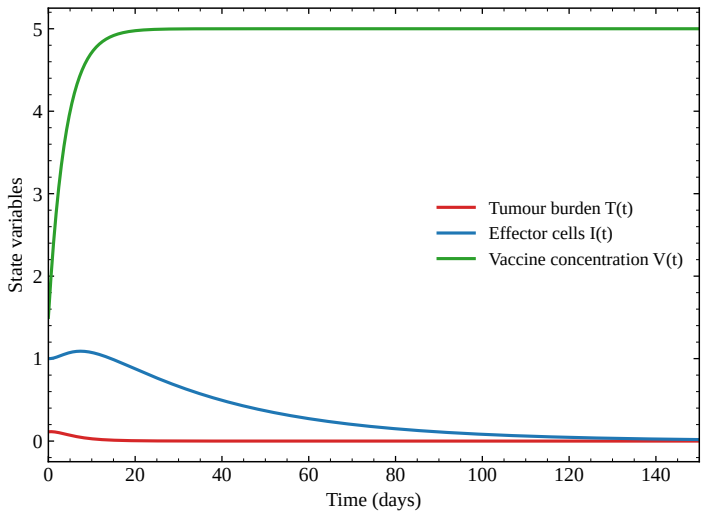


Figure 2. Tumour-free equilibrium for $q = 1$, $\gamma = 0.10$ and $e = 0.25$, giving $\mathcal{R}_T = 0.8500 < 1$ and $\mathcal{R}_I = 0.625 < 1$. Remaining values are the baseline values of Table 1.

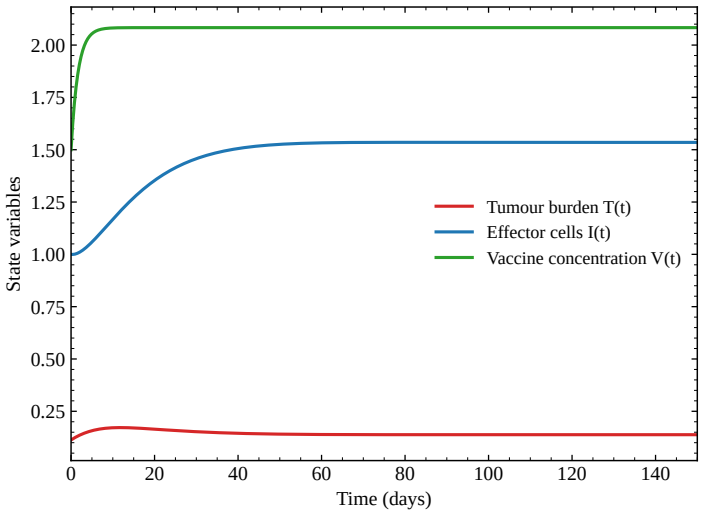


Figure 3. Coexistence equilibrium for $q = 1$ and the baseline values of Table 1, giving $\mathcal{R}_T = 3.8857 > 1$ and $\mathcal{R}_I = 0.625 < 1$.

Remark 2. *Local stability does not by itself exclude chaotic dynamics. For system (3), however, the vaccine equation is linear and decoupled, so $V(t) \to \mu/e$ Lemma 2, and for $q = 1$ the long-term dynamics reduce to a planar system in (T, I). By the Poincaré–Bendixson theorem, such a system cannot be chaotic, and numerical simulations for $q = 0.9$ and 0.7 likewise showed no irregular oscillations.*

5.5. Sensitivity Analysis

The normalized forward sensitivity index of a quantity Q with respect to a parameter p is defined as

$$\Upsilon_p^Q = \frac{p}{Q} \cdot \frac{\partial Q}{\partial p}, \tag{50}$$

so that $\Upsilon_p^Q = +1$ means that a 10% increase in p raises Q by approximately 10%.

5.5.1. Sensitivity of the Threshold Quantities

Since $\mathcal{R}_T = \alpha e/(\gamma\mu)$ and $\mathcal{R}_I = \rho/\eta$ are monomials Equation (50) returns the corresponding exponents:

$$\Upsilon_\alpha^{\mathcal{R}_T} = \Upsilon_e^{\mathcal{R}_T} = +1, \quad \Upsilon_\gamma^{\mathcal{R}_T} = \Upsilon_\mu^{\mathcal{R}_T} = -1, \quad \Upsilon_\rho^{\mathcal{R}_I} = +1, \quad \Upsilon_\eta^{\mathcal{R}_I} = -1. \tag{51}$$

The vaccine parameters therefore act on the invasion threshold only through the ratio μ/e, that is, through the sustained concentration $V^* = \mu/e$. Halving the clearance rate is exactly as effective as doubling the dosing rate. Reducing $\mathcal{R}_T$ below unity from its baseline value 3.886 would require an almost fourfold increase in μ/e or of γ, which confirms quantitatively that vaccination alone is not tumour-eradicating in this parameter regime and that its therapeutic role is to trigger effector recruitment.

5.5.2. Sensitivity of the Residual Tumour Burden

Property 1. *Assume Equation (32). With $\mathcal{N}$, $\mathcal{D}_1$, $\mathcal{D}_2$ and $\mathcal{D}$ as in Equation (26), the indices of T^* are*

$$\begin{aligned} &\Upsilon_\alpha^{T^*} = \frac{\alpha}{\mathcal{N}} - \frac{\mathcal{D}_1}{\mathcal{D}}, \qquad \Upsilon_K^{T^*} = \frac{\mathcal{D}_1}{\mathcal{D}}, \qquad \Upsilon_\gamma^{T^*} = -\frac{\gamma\mu}{e\mathcal{N}}, \\ &\Upsilon_\beta^{T^*} = \Upsilon_\delta^{T^*} = -\frac{\mathcal{D}_2}{\mathcal{D}}, \quad \Upsilon_\mu^{T^*} = -\Upsilon_e^{T^*} = -\frac{\gamma\mu}{e\mathcal{N}} - \frac{\mathcal{D}_2}{\mathcal{D}}, \quad \Upsilon_\eta^{T^*} = -\frac{\eta}{\rho}\Upsilon_\rho^{T^*} = \frac{\eta}{\eta-\rho} \cdot \frac{\mathcal{D}_2}{\mathcal{D}}, \end{aligned} \tag{52}$$

and they satisfy the structural identities

$$\mathrm{Y}_{\alpha}^{T^*} + \mathrm{Y}_{\gamma}^{T^*} + \mathrm{Y}_{K}^{T^*} = 1, \quad \mathrm{Y}_{\mu}^{T^*} = \mathrm{Y}_{\gamma}^{T^*} + \mathrm{Y}_{\beta}^{T^*} = -\mathrm{Y}_{e}^{T^*}, \quad \mathrm{Y}_{\eta}^{T^*} + \mathrm{Y}_{\rho}^{T^*} + \mathrm{Y}_{\beta}^{T^*} = 0. \tag{53}$$

Proof. Taking logarithms in $T^* = \mathcal{N}/\mathcal{D}$ and differentiating,

$$\mathrm{Y}_{p}^{T^*} = \frac{p}{\mathcal{N}}\frac{\partial \mathcal{N}}{\partial p} - \frac{p}{\mathcal{D}}\frac{\partial \mathcal{D}}{\partial p}. \tag{54}$$

From $\mathcal{N} = \alpha - \gamma\mu/e$ one has $p\,\partial_p \mathcal{N} = \alpha, -\gamma\mu/e, -\gamma\mu/e, +\gamma\mu/e$ for $p = \alpha, \gamma, \mu, e$ and 0 otherwise, while from $\mathcal{D} = \mathcal{D}_1 + \mathcal{D}_2$,

$$p\,\frac{\partial \mathcal{D}}{\partial p} = \begin{cases} \mathcal{D}_1, & p = \alpha, \\ -\mathcal{D}_1, & p = K, \\ \mathcal{D}_2, & p \in \{\beta, \delta, \mu\}, \\ -\mathcal{D}_2, & p = e, \\ -\dfrac{\eta}{\eta - \rho}\mathcal{D}_2, & p = \eta, \\ +\dfrac{\rho}{\eta - \rho}\mathcal{D}_2, & p = \rho. \end{cases} \tag{55}$$

Substituting into Equation (54) gives Equation (52). The first identity in Equation (53) follows because the terms $\mathcal{D}_1/\mathcal{D}$ cancel and $(\alpha - \gamma\mu/e)/\mathcal{N} = 1$. The second is immediate. The third follows from $\eta/(\eta - \rho) - \rho/(\eta - \rho) = 1$. □

Table 3 lists these indices for the baseline parameter set of Figure 3, they were checked against central-difference approximations of Equation (50) and agree to all four displayed digits. The effector death rate η is the dominant driver of the residual burden, followed by the effector proliferation rate ρ, the tumour growth rate α and the vaccine pair (μ, e), while β, δ, K and γ play a secondary role. Because $\mathcal{R}_I = 0.625$ is close to unity, small changes in the effector turnover strongly affect the residual burden.

Table 3. Normalized forward sensitivity indices of the residual tumour burden T^*, computed from Equation (52) with the baseline values of Table 1.

Parameter	$\mathbf{Y}_{p}^{T^*}$	Parameter	$\mathbf{Y}_{p}^{T^*}$
η	$+1.4265$	β	-0.5350
ρ	-0.8916	δ	-0.5350
α	$+0.8815$	K	$+0.4650$
e	$+0.8815$	γ	-0.3465
μ	-0.8815		

5.5.3. Sensitivity of the Tumour Burden over the Therapeutic Window

Since the thresholds involve only four parameters and T^* describes only the long-term state, the analysis is completed with the time-dependent index

$$\mathrm{Y}_{p}^{T(t)} = \frac{p}{T(t)}\frac{\partial T(t)}{\partial p}, \tag{56}$$

evaluated at $t = 5$ days, that is, in the early growth phase that precedes the transient peak of the tumour at $t \approx 11.8$ days (Figure 3). The derivatives are approximated by the second-order central difference

$$\frac{\partial T(t)}{\partial p} \simeq \frac{T(t; p + \Delta p) - T(t; p - \Delta p)}{2\Delta p}, \quad \Delta p = 0.01\,p, \tag{57}$$

each solution being generated by the fractional Adams–Bashforth–Moulton predictor–corrector scheme with step $h = 2.5 \times 10^{-3}$ days. At $q = 1$ the scheme reproduces a high-accuracy Runge–Kutta solution of the classical system to seven significant digits, $T(5) = 0.1572517$, and halving h changes the reported indices by less than 10^{-4}. The results are collected in Table 4 and displayed in Figures 4 and 5.

Table 4. Normalized forward sensitivity indices $\Upsilon_p^{T(5)}$ of the tumour burden at $t = 5$ days for the baseline values of Table 1 and different fractional orders. Parameters are ordered by decreasing $|\Upsilon|$ at $q = 1$.

Parameter	$q = 1.00$	$q = 0.95$	$q = 0.90$	$q = 0.85$	$q = 0.80$	Effect of an Increase in p
α	+0.9371	+0.9037	+0.8701	+0.8362	+0.8020	faster growth, larger tumour
K	+0.5116	+0.4902	+0.4687	+0.4473	+0.4259	larger capacity, larger tumour
β	−0.3841	−0.3694	−0.3546	−0.3397	−0.3247	more immune killing, smaller tumour
γ	−0.3453	−0.3307	−0.3162	−0.3018	−0.2874	more vaccine killing, smaller tumour
μ	−0.3010	−0.2836	−0.2665	−0.2497	−0.2334	higher dosing, smaller tumour
e	+0.2702	+0.2541	+0.2383	+0.2228	+0.2077	faster clearance, larger tumour
η	+0.0816	+0.0767	+0.0719	+0.0671	+0.0624	faster effector death, larger tumour
ρ	−0.0510	−0.0480	−0.0449	−0.0420	−0.0390	more effector expansion, smaller tumour
δ	−0.0394	−0.0371	−0.0347	−0.0323	−0.0300	more recruitment, smaller tumour
$T(5)$ (mL)	0.157252	0.155119	0.153038	0.151007	0.149028	

Figure 4 presents the normalized sensitivity indices of the tumour burden at $t = 5$ days for $q = 1$. The most influential parameters are the intrinsic tumour growth rate α (+0.9371), the carrying capacity K (+0.5116), and the immune-mediated tumour clearance rate β (−0.3841). A local linear approximation indicates that a 10% increase in α yields approximately a 9.4% increase in $T(5)$. Positive indices for α, K, e, and η imply that increasing these parameters elevates the tumour burden, whereas negative indices for β, γ, μ, ρ, and δ indicate tumour suppression. The vaccine parameters γ, μ, and e exhibit moderate sensitivity, while the effector rates η and ρ and the activation rate δ have the smallest effect during this early phase, because the effector population has not yet changed appreciably from its initial value.

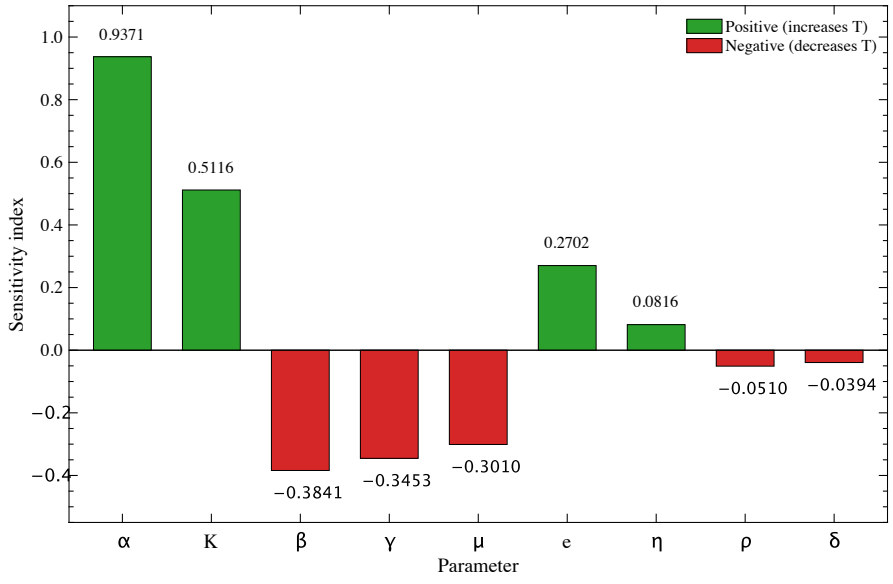


Figure 4. Normalized forward sensitivity indices of the tumour burden $T(5)$ with respect to the model parameters for $q = 1$.

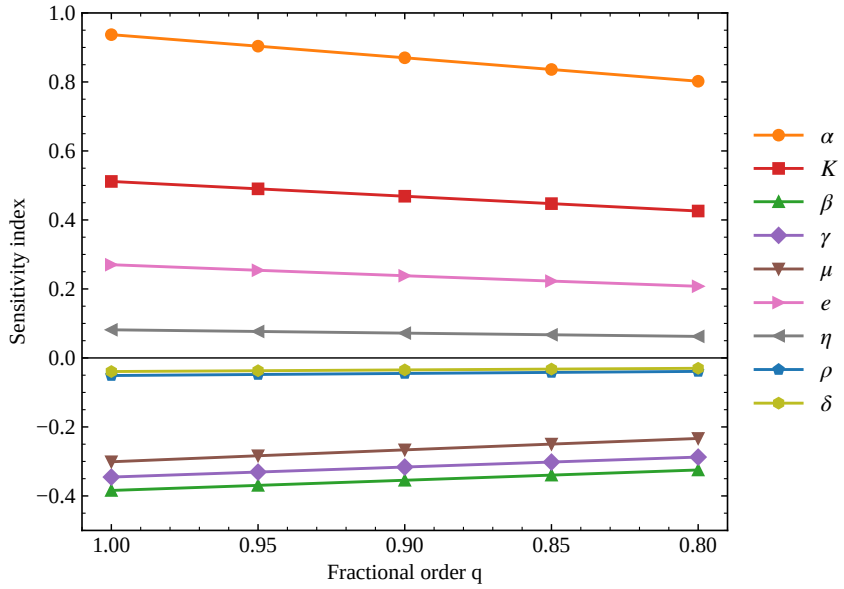


Figure 5. Variation in the sensitivity indices $\Upsilon_p^{T(5)}$ with different fractional order q = 1.0, 0.95, 0.9, 0.85, and 0.8.

Figure 5 illustrates an approximately linear decline of 14.4–23.8% in the sensitivity magnitudes as q decreases from 1 to 0.8, with their signs unchanged and relative ranking preserved. Concurrently, $T(5)$ decreases from 0.157252 mL to 0.149028 mL, indicating that memory effects slow the early tumour growth at the observation time for lower fractional orders.

6. Yang Transform Adomian Decomposition Method (YTADM)

We consider a general nonlinear fractional differential equation of the form

$$^{C}D_t^q\Theta(t) = \mathscr{L}\Theta(t) + \mathscr{N}\Theta(t) + g(t), \quad t \geq 0, \tag{58}$$

subject to the initial condition $\Theta(0) = \Theta_0$, where $0 < q \leq 1$, $\mathscr{L}$ is a linear operator, $\mathscr{N}$ is a nonlinear operator, and $g(t)$ is a known source term. Utilizing the Yang transform to Equation (58), we have

$$\begin{aligned} \frac{\Theta(\chi)}{\chi^q} - \frac{\Theta(0)}{\chi^{q-1}} &= \Upsilon\left[g(t) + \mathscr{L}\Theta(t) + \mathscr{N}\Theta(t)\right] \\ \Theta(\chi) &= \chi\Theta_0 + \chi^q\Upsilon\left[g(t) + \mathscr{L}\Theta(t) + \mathscr{N}\Theta(t)\right]. \end{aligned} \tag{59}$$

Applying the inverse Yang transform to Equation (59), we have

$$\Theta(t) = \Theta_0 + \Upsilon^{-1}\left[\chi^q\Upsilon\left[g(t) + \mathscr{L}\Theta(t) + \mathscr{N}\Theta(t)\right]\right]. \tag{60}$$

Assume that

$$\Theta(t) = \sum_{n=0}^{\infty}\Theta_n(t), \quad \mathscr{N}\Theta(t) = \sum_{n=0}^{\infty}\mathcal{B}_n, \tag{61}$$

Substituting Equation (61) into Equation (60) yields the recursive scheme

$$\begin{cases} \Theta_0(t) & = \Theta(0) + \mathsf{Y}^{-1}\Big[\chi^q \mathsf{Y}\Big[g(t)\Big]\Big] \\ \vdots & \\ \Theta_{n+1}(t) & = \mathsf{Y}^{-1}\Big[\chi^q \mathsf{Y}\Big[\mathscr{L}(\Theta_n) + \mathcal{B}_n\Big]\Big], \quad n \geq 0. \end{cases} \tag{62}$$

Therefore, the YTADM solution is given by

$$\Theta(t) = \sum_{n=0}^{\infty} \Theta_n(t) = \Theta_0(t) + \Theta_1(t) + \Theta_2(t) + \cdots. \tag{63}$$

7. Application to the Tumour–Immune–Vaccine Model

In this section, the YTADM is applied to the fractional system (3) to obtain approximate series solutions for the tumour burden, effector cells and vaccine concentration. Applying the Yang transform to each equation of system (3), we obtain

$$\begin{aligned} \mathsf{Y}\Big[{}^{C}D_t^q T(t)\Big] &= \mathsf{Y}\Big[\alpha T\Big(1 - \frac{T}{K}\Big) - \beta IT - \gamma VT\Big], \\ \mathsf{Y}\Big[{}^{C}D_t^q I(t)\Big] &= \mathsf{Y}\Big[\delta VT + \rho I - \eta I\Big], \\ \mathsf{Y}\Big[{}^{C}D_t^q V(t)\Big] &= \mathsf{Y}\Big[\mu - eV\Big], \end{aligned} \tag{64}$$

and

$$\begin{aligned} \frac{\mathsf{T}(\chi)}{\chi^q} - \frac{T(0)}{\chi^{q-1}} &= \mathsf{Y}\Big[\alpha T - \frac{\alpha}{K}T^2 - \beta IT - \gamma VT\Big], \\ \frac{\mathsf{I}(\chi)}{\chi^q} - \frac{I(0)}{\chi^{q-1}} &= \mathsf{Y}\Big[\delta VT + (\rho - \eta)I\Big], \\ \frac{\mathsf{V}(\chi)}{\chi^q} - \frac{V(0)}{\chi^{q-1}} &= \mathsf{Y}\Big[\mu - eV\Big]. \end{aligned} \tag{65}$$

Simplifying and using the initial conditions of Equation (2), we have

$$\begin{aligned} \mathsf{T}(\chi) &= 0.113\chi + \chi^q \mathsf{Y}\Big[\alpha T - \frac{\alpha}{K}T^2 - \beta IT - \gamma VT\Big], \\ \mathsf{I}(\chi) &= 1.0\chi + \chi^q \mathsf{Y}\Big[\delta VT + (\rho - \eta)I\Big], \\ \mathsf{V}(\chi) &= 1.5\chi + \chi^q \mathsf{Y}\Big[\mu - eV\Big]. \end{aligned} \tag{66}$$

Applying the inverse Yang transform to Equation (66), we have

$$\begin{aligned} T(t) &= 0.113 + \mathsf{Y}^{-1}\Big[\chi^q \mathsf{Y}\Big\{\alpha T - \frac{\alpha}{K}T^2 - \beta IT - \gamma VT\Big\}\Big], \\ I(t) &= 1.000 + \mathsf{Y}^{-1}\Big[\chi^q \mathsf{Y}\Big\{\delta VT + (\rho - \eta)I\Big\}\Big], \\ V(t) &= 1.500 + \mathsf{Y}^{-1}\Big[\chi^q \mathsf{Y}\Big\{\mu - eV\Big\}\Big]. \end{aligned} \tag{67}$$

Assume that the solutions are expressed as the series

$$T(t) = \sum_{n=0}^{\infty} T_n(t), \quad I(t) = \sum_{n=0}^{\infty} I_n(t), \quad V(t) = \sum_{n=0}^{\infty} V_n(t), \tag{68}$$

and the nonlinear terms are decomposed as

$$T^2 = \sum_{n=0}^{\infty} \mathcal{A}_n, \quad IT = \sum_{n=0}^{\infty} \mathcal{B}_n, \quad VT = \sum_{n=0}^{\infty} \mathcal{C}_n, \tag{69}$$

where $\mathcal{A}_n, \mathcal{B}_n, \mathcal{C}_n$ are defined as

$$\begin{aligned} &\mathcal{A}_0 = T_0^2, && \mathcal{B}_0 = I_0 T_0, && \mathcal{C}_0 = V_0 T_0, \\ &\mathcal{A}_1 = 2T_0 T_1, && \mathcal{B}_1 = I_0 T_1 + I_1 T_0, && \mathcal{C}_1 = V_0 T_1 + V_1 T_0, \\ &\mathcal{A}_2 = 2T_0 T_2 + T_1^2, && \mathcal{B}_2 = I_0 T_2 + I_1 T_1 + I_2 T_0, && \mathcal{C}_2 = V_0 T_2 + V_1 T_1 + V_2 T_0. \end{aligned} \tag{70}$$

Substituting Equations (68) and (69) into Equation (67) gives the recursive scheme

$$\begin{aligned} T_{n+1}(t) &= \mathsf{Y}^{-1}\left[\chi^q \mathsf{Y}\left\{\alpha T_n - \frac{\alpha}{K}\mathcal{A}_n - \beta \mathcal{B}_n - \gamma C_n\right\}\right], \\ I_{n+1}(t) &= \mathsf{Y}^{-1}\left[\chi^q \mathsf{Y}\left\{\delta \mathcal{C}_n + (\rho - \eta) I_n\right\}\right], \\ V_{n+1}(t) &= \mathsf{Y}^{-1}\left[\chi^q \mathsf{Y}\left\{\mu - e V_n\right\}\right], \quad n \geq 0. \end{aligned} \tag{71}$$

Remark 3. *The YTADM does not require zero initial values. The initial values (2) enter only as the zeroth components in (67), and non-zero values feed the Adomian polynomials (70), whereas zero values remove them. For $T(0) = 0$, the series reduces to the exact tumour-free solution.*

For $n = 0$, we have

$$\begin{aligned} T_1(t) &= \mathsf{Y}^{-1}\left[\chi^q \mathsf{Y}\left\{\alpha T_0 - \frac{\alpha}{K}\mathcal{A}_0 - \beta \mathcal{B}_0 - \gamma C_0\right\}\right], \\ I_1(t) &= \mathsf{Y}^{-1}\left[\chi^q \mathsf{Y}\left\{\delta \mathcal{C}_0 + (\rho - \eta) I_0\right\}\right], \\ V_1(t) &= \mathsf{Y}^{-1}\left[\chi^q \mathsf{Y}\left\{\mu - e V_0\right\}\right]. \end{aligned} \tag{72}$$

$$\begin{aligned} T_1(t) &= \mathsf{Y}^{-1}\left[\chi^q \mathsf{Y}\left\{0.048025 - 0.013567 - 0.012430 - 0.008899\right\}\right], \\ I_1(t) &= \mathsf{Y}^{-1}\left[\chi^q \mathsf{Y}\left\{0.027120 - 0.030000\right\}\right], \\ V_1(t) &= \mathsf{Y}^{-1}\left[\chi^q \mathsf{Y}\left\{1.250 - 0.900\right\}\right]. \end{aligned} \tag{73}$$

$$\begin{aligned} T_1(t) &= \mathsf{Y}^{-1}\left[\chi^q \,\mathsf{Y}\left\{0.013129\right\}\right], \\ I_1(t) &= \mathsf{Y}^{-1}\left[\chi^q \,\mathsf{Y}\left\{-0.002880\right\}\right], \\ V_1(t) &= \mathsf{Y}^{-1}\left[\chi^q \,\mathsf{Y}\left\{0.350000\right\}\right]. \end{aligned} \tag{74}$$

Applying the Yang inverse transform to Equation (74), we have

$$\begin{aligned} T_1(t) &= 0.013129\,\frac{t^q}{\Gamma(q+1)} \\ I_1(t) &= -0.002880\,\frac{t^q}{\Gamma(q+1)} \\ V_1(t) &= 0.350000\,\frac{t^q}{\Gamma(q+1)}. \end{aligned} \tag{75}$$

For $n = 1$, we have

$$\begin{aligned} T_2(t) &= \mathrm{Y}^{-1}\left[\chi^q \mathrm{Y}\left\{\alpha T_1 - \frac{\alpha}{K}\mathcal{A}_1 - \beta\mathcal{B}_1 - \gamma C_1\right\}\right], \\ I_2(t) &= \mathrm{Y}^{-1}\left[\chi^q \mathrm{Y}\left\{\delta\mathcal{C}_1 + (\rho-\eta)I_1\right\}\right], \\ V_2(t) &= \mathrm{Y}^{-1}\left[\chi^q \mathrm{Y}\left\{-eV_1\right\}\right]. \end{aligned} \tag{76}$$

$$\begin{aligned} T_2(t) &= \mathrm{Y}^{-1}\left[\chi^q \mathrm{Y}\left\{\left[0.005580 - 0.003153 - 0.001408 - 0.003110\right]\frac{t^q}{\Gamma(q+1)}\right\}\right], \\ I_2(t) &= \mathrm{Y}^{-1}\left[\chi^q \mathrm{Y}\left\{\left[0.009479 + 0.000086\right]\frac{t^q}{\Gamma(q+1)}\right\}\right], \\ V_2(t) &= \mathrm{Y}^{-1}\left[\chi^q \mathrm{Y}\left\{-(0.600)(0.350000)\,\frac{t^q}{\Gamma(q+1)}\right\}\right]. \end{aligned} \tag{77}$$

$$\begin{aligned} T_2(t) &= \mathrm{Y}^{-1}\left[\chi^q \mathrm{Y}\left\{-0.002091\frac{t^q}{\Gamma(q+1)}\right\}\right], \\ I_2(t) &= \mathrm{Y}^{-1}\left[\chi^q \mathrm{Y}\left\{0.009565\,\frac{t^q}{\Gamma(q+1)}\right\}\right], \\ V_2(t) &= \mathrm{Y}^{-1}\left[\chi^q \mathrm{Y}\left\{-0.210000\frac{t^q}{\Gamma(q+1)}\right\}\right]. \end{aligned} \tag{78}$$

Applying the inverse Yang transform to Equation (78), we have

$$\begin{aligned} T_2(t) &= -0.002091\frac{t^{2q}}{\Gamma(2q+1)}, \\ I_2(t) &= 0.009565\frac{t^{2q}}{\Gamma(2q+1)}, \\ V_2(t) &= -0.210000\frac{t^{2q}}{\Gamma(2q+1)}. \end{aligned} \tag{79}$$

For $n = 2$, we have

$$\begin{aligned} T_3(t) &= \mathrm{Y}^{-1}\left[\chi^q \mathrm{Y}\left\{\alpha T_2 - \frac{\alpha}{K}\mathcal{A}_2 - \beta\mathcal{B}_2 - \gamma C_2\right\}\right], \\ I_3(t) &= \mathrm{Y}^{-1}\left[\chi^q \mathrm{Y}\left\{\delta\mathcal{C}_2 + (\rho-\eta)I_2\right\}\right], \\ V_3(t) &= \mathrm{Y}^{-1}\left[\chi^q \mathrm{Y}\left\{-eV_2\right\}\right]. \end{aligned} \tag{80}$$

$$
\begin{aligned}
T_3(t) &= \mathsf{Y}^{-1}\left[\chi^q\mathsf{Y}\left\{0.425\left(-0.002091\frac{t^{2q}}{\Gamma(2q+1)}\right)-1.0625\left(-0.000473\frac{t^{2q}}{\Gamma(2q+1)}+0.000172\frac{t^{2q}}{\Gamma(q+1)^2}\right)\right.\right.\\
&\quad\left.\left.-0.110\left(-0.001011\frac{t^{2q}}{\Gamma(2q+1)}-0.000038\frac{t^{2q}}{\Gamma(q+1)^2}\right)-0.0525\left(-0.026867\frac{t^{2q}}{\Gamma(2q+1)}+0.004595\frac{t^{2q}}{\Gamma(q+1)^2}\right)\right\}\right],\\
I_3(t) &= \mathsf{Y}^{-1}\left[\chi^q\mathsf{Y}\left\{0.160\left(-0.026867\frac{t^{2q}}{\Gamma(2q+1)}+0.004595\frac{t^{2q}}{\Gamma(q+1)^2}\right)-0.030\left(0.009565\frac{t^{2q}}{\Gamma(2q+1)}\right)\right\}\right],\\
V_3(t) &= \mathsf{Y}^{-1}\left[\chi^q\mathsf{Y}\left\{-0.600\left(-0.210000\frac{t^{2q}}{\Gamma(2q+1)}\right)\right\}\right].
\end{aligned}
\tag{81}
$$

$$
\begin{aligned}
T_3(t) &= \mathsf{Y}^{-1}\left[\chi^q\mathsf{Y}\left\{\left[-0.000889+0.000502+0.000111+0.001411\right]\frac{t^{2q}}{\Gamma(2q+1)}\right.\right.\\
&\quad\left.\left.+\left[-0.000183+0.000004-0.000241\right]\frac{t^{2q}}{\Gamma(q+1)^2}\right\}\right],\\
I_3(t) &= \mathsf{Y}^{-1}\left[\chi^q\mathsf{Y}\left\{\left[-0.004299-0.000287\right]\frac{t^{2q}}{\Gamma(2q+1)}+0.000735\frac{t^{2q}}{\Gamma(q+1)^2}\right\}\right],\\
V_3(t) &= \mathsf{Y}^{-1}\left[\chi^q\mathsf{Y}\left\{0.126000\frac{t^{2q}}{\Gamma(2q+1)}\right\}\right],
\end{aligned}
\tag{82}
$$

$$
\begin{aligned}
T_3(t) &= \mathsf{Y}^{-1}\left[\chi^q\mathsf{Y}\left\{0.001135\frac{t^{2q}}{\Gamma(2q+1)}-0.000420\frac{t^{2q}}{\Gamma(q+1)^2}\right\}\right],\\
I_3(t) &= \mathsf{Y}^{-1}\left[\chi^q\mathsf{Y}\left\{-0.004586\frac{t^{2q}}{\Gamma(2q+1)}+0.000735\,\frac{t^{2q}}{\Gamma(q+1)^2}\right\}\right],\\
V_3(t) &= \mathsf{Y}^{-1}\left[\chi^q\mathsf{Y}\left\{0.126000\frac{t^{2q}}{\Gamma(2q+1)}\right\}\right].
\end{aligned}
\tag{83}
$$

Applying the inverse Yang transform to Equation (83), we have

$$
\begin{aligned}
T_3(t) &= \left[0.001135-0.000420\frac{\Gamma(2q+1)}{\Gamma(q+1)^2}\right]\frac{t^{3q}}{\Gamma(3q+1)},\\
I_3(t) &= \left[-0.004586+0.000735\,\frac{\Gamma(2q+1)}{\Gamma(q+1)^2}\right]\frac{t^{3q}}{\Gamma(3q+1)},\\
V_3(t) &= 0.126000\,\frac{t^{3q}}{\Gamma(3q+1)}.
\end{aligned}
\tag{84}
$$

Therefore, the YTADM solution is given by

$$
\begin{cases}
T(t) = 0.113+0.013129\,\dfrac{t^q}{\Gamma(q+1)}-0.002091\,\dfrac{t^{2q}}{\Gamma(2q+1)}+\left[0.001135-0.000420\dfrac{\Gamma(2q+1)}{\Gamma(q+1)^2}\right]\dfrac{t^{3q}}{\Gamma(3q+1)}+\cdots\\
I(t) = 1.0-0.002880\dfrac{t^q}{\Gamma(q+1)}+0.009565\,\dfrac{t^{2q}}{\Gamma(2q+1)}+\left[-0.004586+0.000735\dfrac{\Gamma(2q+1)}{\Gamma(q+1)^2}\right]\dfrac{t^{3q}}{\Gamma(3q+1)}+\cdots\\
V(t) = 1.5+0.350000\dfrac{t^q}{\Gamma(q+1)}-0.210000\dfrac{t^{2q}}{\Gamma(2q+1)}+0.126000\dfrac{t^{3q}}{\Gamma(3q+1)}+\cdots.
\end{cases}
\tag{85}
$$

Tables 5–7 present the YTADM approximation (85) for different fractional orders. The tumour burden and vaccine concentration increase over the first two days, while the effector population decreases slightly before increasing. Table 8 compares the YTADM and Runge–Kutta solutions for $q = 1$ and shows close agreement, with differences below 10^{-6} for all three variables over $0 \le t \le 2$.

For $0 < q < 1$, Tables 9 and 10 compare the YTADM solution with the fractional Adams–Bashforth–Moulton method. The four-term solution (85) is accurate to 0.3% for T and I, but its error in V reaches 5% at $t = 2$ for $q = 0.6$. With $N = 10$ terms, all errors fall below 2.5×10^{-4}, and these terms are used in Tables 5–8 and Figures 6–10.

Figures 6 and 7a show that smaller fractional orders produce a faster initial increase in tumour burden and vaccine concentration, followed by a slower increase later in the interval. Consequently, the tumour curves intersect between $t \approx 1.08$ and 1.34 days and the vaccine curves between $t \approx 0.83$ and 1.03 days, whereas the effector curves intersect early, between $t \approx 0.07$ and 0.22 days, and for $q \leq 0.8$ again at about 1.7–1.9 days. The effector minimum occurs earlier and is slightly shallower as q decreases.

Table 5. Tumour burden $T(t)$ in mL for different fractional orders of YTADM solution (85).

t	$q = 1.00$	$q = 0.90$	$q = 0.80$	$q = 0.70$	$q = 0.60$
0.01	0.113131	0.113216	0.113353	0.113573	0.113920
0.05	0.113654	0.113915	0.114271	0.114750	0.115384
0.10	0.114303	0.114699	0.115198	0.115818	0.116576
1.00	0.125131	0.125484	0.125759	0.125947	0.126042
2.00	0.135434	0.134606	0.133696	0.132713	0.131663

Table 6. Effector cell population $I(t)$ in millions of cells for different fractional orders of YTADM solution (85).

t	$q = 1.00$	$q = 0.90$	$q = 0.80$	$q = 0.70$	$q = 0.60$
0.01	0.999972	0.999954	0.999927	0.999886	0.999831
0.05	0.999868	0.999824	0.999773	0.999724	0.999695
0.10	0.999759	0.999712	0.999674	0.999662	0.999706
1.00	1.001416	1.002004	1.002611	1.003205	1.003752
2.00	1.009734	1.010050	1.010147	1.010019	1.009672

Table 7. Vaccine concentration $V(t)$ in mg/mL for different fractional orders of YTADM solution (85).

t	$q = 1.00$	$q = 0.90$	$q = 0.80$	$q = 0.70$	$q = 0.60$
0.01	1.503490	1.505736	1.509347	1.515070	1.523975
0.05	1.517240	1.523990	1.533021	1.544863	1.560005
0.10	1.533971	1.543888	1.556030	1.570557	1.587465
1.00	1.763193	1.763979	1.763026	1.760564	1.756850
2.00	1.907638	1.886398	1.865757	1.845799	1.826587

Table 8. Comparison of the YTADM solution (85) and Runge–Kutta solutions for the tumour–immune–vaccine model with $q = 1$.

t	$T(t)$ (mL)		$I(t)$ (Million Cells)		$V(t)$ (mg/mL)	
	YTADM	RK	YTADM	RK	YTADM	RK
0.01	0.1131312	0.1131312	0.9999717	0.9999717	1.5034895	1.5034895
0.03	0.1133929	0.1133929	0.9999179	0.9999179	1.5104061	1.5104061
0.05	0.1136539	0.1136539	0.9998679	0.9998679	1.5172401	1.5172401
0.07	0.1139139	0.1139139	0.9998217	0.9998217	1.5239926	1.5239926
0.10	0.1143025	0.1143025	0.9997593	0.9997593	1.5339707	1.5339707
0.50	0.1193092	0.1193092	0.9996928	0.9996928	1.6511894	1.6511894
1.00	0.1251307	0.1251307	1.0014161	1.0014161	1.7631932	1.7631932
1.50	0.1304965	0.1304965	1.0048535	1.0048535	1.8461678	1.8461677
2.00	0.1354342	0.1354342	1.0097343	1.0097343	1.9076376	1.9076367

Table 9. Comparison of the YTADM solution (85) with the fractional Adams–Bashforth–Moulton (ABM) solution ($h = 10^{-4}$) for $0 < q < 1$. $E_X = |X_{\text{YTADM}} - X_{\text{ABM}}|$.

q	t	$T(t)$ (mL)			$I(t)$ (Million Cells)			$V(t)$ (mg/mL)		
		YTADM	ABM	E_T	YTADM	ABM	E_I	YTADM	ABM	E_V
0.9	0.1	0.114699	0.114699	1.78×10^{-8}	0.999712	0.999712	2.32×10^{-8}	1.543889	1.543888	1.39×10^{-6}
	0.5	0.119971	0.119970	7.40×10^{-7}	0.999914	0.999920	6.25×10^{-6}	1.663694	1.663264	4.30×10^{-4}
	1.0	0.125493	0.125484	9.21×10^{-6}	1.001931	1.002004	7.33×10^{-5}	1.768863	1.763979	4.88×10^{-3}
	1.5	0.130343	0.130304	3.88×10^{-5}	1.005192	1.005499	3.07×10^{-4}	1.854579	1.834768	1.98×10^{-2}
	2.0	0.134713	0.134606	1.07×10^{-4}	1.009210	1.010050	8.40×10^{-4}	1.939213	1.886393	5.28×10^{-2}
0.8	0.1	0.115198	0.115198	7.53×10^{-9}	0.999673	0.999674	1.07×10^{-7}	1.556036	1.556030	5.96×10^{-6}
	0.5	0.120642	0.120639	2.65×10^{-6}	1.000217	1.000233	1.65×10^{-5}	1.675383	1.674430	9.53×10^{-4}
	1.0	0.125782	0.125759	2.34×10^{-5}	1.002466	1.002611	1.44×10^{-4}	1.771158	1.763025	8.13×10^{-3}
	1.5	0.130092	0.130010	8.19×10^{-5}	1.005528	1.006033	5.06×10^{-4}	1.850588	1.822643	2.79×10^{-2}
	2.0	0.133893	0.133697	1.97×10^{-4}	1.008924	1.010146	1.22×10^{-3}	1.932062	1.865738	6.63×10^{-2}
0.7	0.1	0.115818	0.115818	6.07×10^{-8}	0.999662	0.999662	4.78×10^{-7}	1.570581	1.570557	2.43×10^{-5}
	0.5	0.121310	0.121303	7.33×10^{-6}	1.000597	1.000637	3.94×10^{-5}	1.686426	1.684417	2.01×10^{-3}
	1.0	0.125995	0.125947	4.78×10^{-5}	1.002947	1.003205	2.58×10^{-4}	1.773467	1.760563	1.29×10^{-2}
	1.5	0.129758	0.129618	1.40×10^{-4}	1.005664	1.006427	7.63×10^{-4}	1.847713	1.810075	3.76×10^{-2}
	2.0	0.133012	0.132713	2.98×10^{-4}	1.008383	1.010016	1.63×10^{-3}	1.925395	1.845726	7.97×10^{-2}
0.6	0.1	0.116576	0.116576	3.77×10^{-7}	0.999704	0.999706	2.01×10^{-6}	1.587559	1.587465	9.39×10^{-5}
	0.5	0.121963	0.121946	1.74×10^{-5}	1.001040	1.001127	8.64×10^{-5}	1.697054	1.693050	4.00×10^{-3}
	1.0	0.126127	0.126042	8.50×10^{-5}	1.003328	1.003752	4.24×10^{-4}	1.776271	1.756846	1.94×10^{-2}
	1.5	0.129341	0.129129	2.11×10^{-4}	1.005591	1.006654	1.06×10^{-3}	1.845484	1.797264	4.82×10^{-2}
	2.0	0.132065	0.131665	4.00×10^{-4}	1.007640	1.009666	2.03×10^{-3}	1.917559	1.826344	9.12×10^{-2}

Table 10. Maximum absolute error $\max_{0 \le t \le 2} |X^{(N)}_{\text{YTADM}} - X_{\text{ABM}}|$ of the YTADM solution (85).

N	Variable	$q = 1.0$	$q = 0.9$	$q = 0.8$	$q = 0.7$	$q = 0.6$
4	T	3.40×10^{-5}	1.05×10^{-4}	1.95×10^{-4}	2.97×10^{-4}	3.99×10^{-4}
	I	5.17×10^{-4}	8.38×10^{-4}	1.22×10^{-3}	1.63×10^{-3}	2.02×10^{-3}
	V	4.04×10^{-2}	5.28×10^{-2}	6.63×10^{-2}	7.97×10^{-2}	9.12×10^{-2}
6	T	1.12×10^{-5}	1.16×10^{-5}	6.14×10^{-6}	9.98×10^{-6}	4.06×10^{-5}
	I	3.43×10^{-5}	2.70×10^{-5}	7.12×10^{-6}	8.52×10^{-5}	2.20×10^{-4}
	V	2.06×10^{-3}	3.92×10^{-3}	7.00×10^{-3}	1.16×10^{-2}	1.78×10^{-2}
8	T	6.21×10^{-7}	1.64×10^{-6}	3.26×10^{-6}	4.85×10^{-6}	4.36×10^{-6}
	I	2.81×10^{-6}	6.38×10^{-6}	1.13×10^{-5}	1.44×10^{-5}	7.19×10^{-6}
	V	5.48×10^{-5}	1.63×10^{-4}	4.41×10^{-4}	1.09×10^{-3}	2.40×10^{-3}
10	T	2.42×10^{-8}	7.23×10^{-9}	1.85×10^{-7}	6.93×10^{-7}	1.61×10^{-6}
	I	3.94×10^{-8}	1.50×10^{-7}	9.06×10^{-7}	2.80×10^{-6}	5.75×10^{-6}
	V	8.97×10^{-7}	4.35×10^{-6}	1.89×10^{-5}	7.27×10^{-5}	2.43×10^{-4}

The phase portraits in Figures 7b and 8 show the relationships between the three state variables. At $t = 2$ days, smaller fractional orders yield lower tumour burdens and vaccine concentrations, whereas the effector population is not monotone in q. Figures 9 and 10 display the solutions as functions of time and fractional order. Over the plotted interval, the effector population changes by about 1% of its initial value, whereas the tumour burden and vaccine concentration increase by approximately 16–20% and 22–27%, respectively.

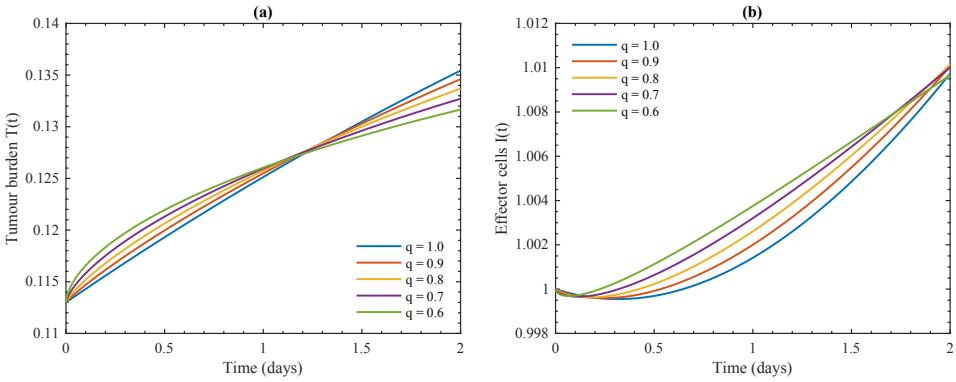


Figure 6. YTADM solution (85): (**a**) the tumour burden $T(t)$ and (**b**) the effector cells $I(t)$ for $0.6 \leq q \leq 1$.

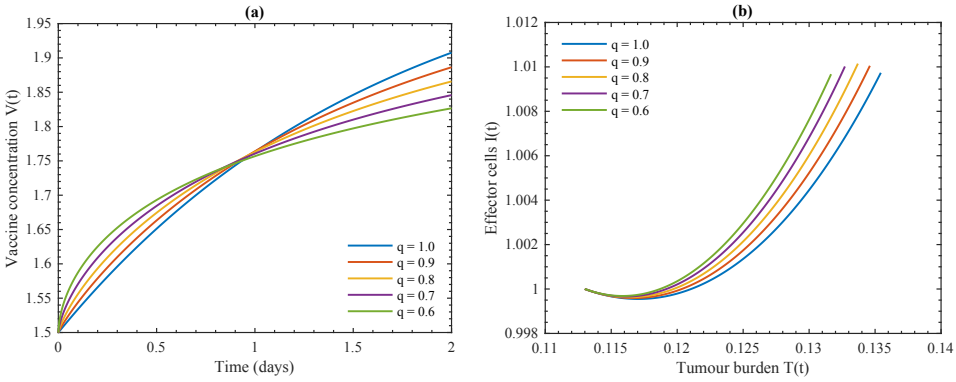


Figure 7. YTADM solution (85): (**a**) the vaccine concentration $V(t)$ and (**b**) the (T, I) phase portrait for $0.6 \leq q \leq 1$.

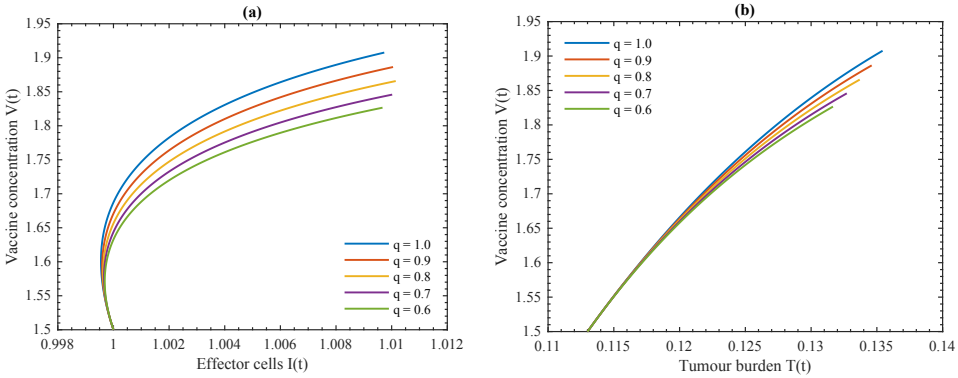


Figure 8. YTADM solution (85): (**a**) the phase portrait V versus I and (**b**) the phase portrait V versus T for $0.6 \leq q \leq 1$.

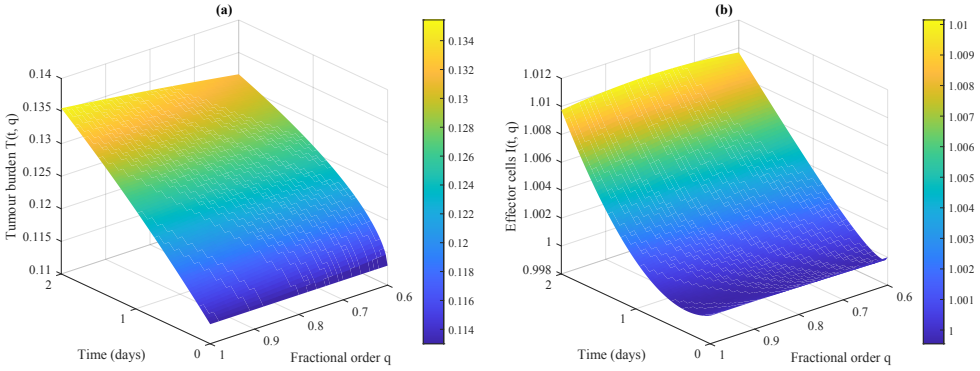


Figure 9. 3-D surfaces of (**a**) the tumour burden $T(t, q)$ and (**b**) the effector cell population $I(t, q)$ obtained from the YTADM solution (85) for $0.6 \leq q \leq 1$.

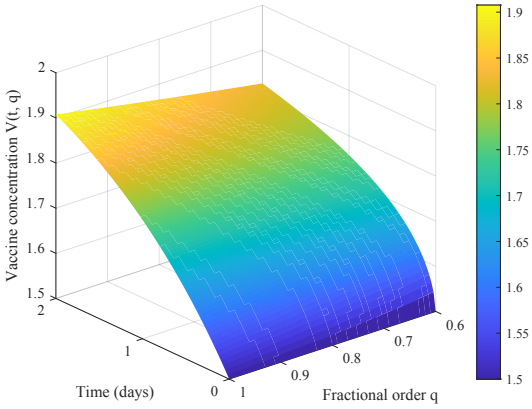


Figure 10. 3-D surface of the vaccine concentration $V(t, q)$ obtained from the YTADM solution (85) for $0.6 \leq q \leq 1$.

8. Conclusions

In this study, the tumour–immune–vaccine model was extended to a Caputo fractional-order framework, and its stability, sensitivity and semi-analytical solutions were investigated. The solutions were shown to remain non-negative, with the tumour burden bounded by the carrying capacity. For $\eta > \rho$, the effector population is uniformly bounded and solutions are attracted to a compact feasible region, whereas for $\eta \leq \rho$ only bounds on finite time intervals hold. The vaccine concentration was obtained in closed form. Two threshold quantities, the tumour invasion number $\mathcal{R}_T$ and the effector self-renewal number $\mathcal{R}_I$, govern the local stability of the equilibria. The tumour-free equilibrium is locally asymptotically stable when both are below unity. When $\mathcal{R}_T$ exceeds unity and $\mathcal{R}_I$ remains below it, tumour and immune cells coexist at a locally asymptotically stable equilibrium. These stability conditions do not depend on the fractional order. In the degenerate case $\mathcal{R}_I = 1$, there are infinitely many tumour-free equilibria, none of which is asymptotically stable.

For the baseline parameters, the model predicts a stable coexistence state with a small residual tumour burden. The sensitivity analysis shows that the effector death and proliferation rates control this residual burden, whereas the tumour growth rate and carrying capacity dominate the tumour burden during the early therapeutic window. Because $\mathcal{R}_T$ depends only on the tumour growth rate and the vaccine parameters, immune recruitment cannot by itself shift the system to the tumour-free state. Eliminating the tumour would require an almost fourfold increase in the sustained vaccine level or in the vaccine killing rate. In this regime, the main benefit of vaccination is to stimulate effector recruitment, which lowers the residual tumour burden.

The Yang transform Adomian decomposition method provided explicit series solutions, which were validated against Runge–Kutta solutions for $q = 1$ and against the fractional Adams–Bashforth–Moulton method for $0 < q < 1$. Fractional memory produces a faster initial increase in tumour burden and vaccine concentration, followed by slower subsequent growth. At $t = 5$ days, decreasing the fractional order from 1 to 0.8 reduced the magnitude of every sensitivity index by 14.4–23.9% without changing their signs.

The model is not fitted to clinical data, and the series solution is accurate only over short time intervals. Future work may include fitting the model to patient data, extending the solution to longer times, and studying optimal vaccine schedules within the fractional framework.

Author Contributions: M.A.A., conceptualization, methodology, software, validation, formal analysis, investigation, writing—original draft preparation and writing—review and editing; M.M.,

methodology, validation, resources, writing—review and editing, visualization and supervision; M.A.F., validation and writing—review and editing. All authors have read and agreed to the published version of the manuscript.

Funding: For this manuscript no funding was received.

Data Availability Statement: Data is contained within the article.

Conflicts of Interest: The authors declare no conflicts of interest.

References

1. Kuznetsov, V.A.; Makalkin, I.A.; Taylor, M.A.; Perelson, A.S. Nonlinear dynamics of immunogenic tumors: Parameter estimation and global bifurcation analysis. *Bull. Math. Biol.* **1994**, *56*, 295–321. https://doi.org/10.1007/BF02460644.
2. Kirschner, D.; Panetta, J.C. Modeling immunotherapy of the tumor–immune interaction. *J. Math. Biol.* **1998**, *37*, 235–252. https://doi.org/10.1007/s002850050127.
3. de Pillis, L.G.; Radunskaya, A.E. A mathematical model of immune response to tumor invasion. In *Computational Fluid and Solid Mechanics 2003*; Bathe, K.J., Ed.; Elsevier Science: Amsterdam, The Netherlands, 2003; pp. 1661–1668. https://doi.org/10.1016/B978-008044046-0.50404-8.
4. de Pillis, L.G.; Radunskaya, A.E.; Wiseman, C.L. A validated mathematical model of cell-mediated immune response to tumor growth. *Cancer Res.* **2005**, *65*, 7950–7958.
5. de Pillis, L.G.; Gu, W.; Radunskaya, A.E. Mixed immunotherapy and chemotherapy of tumors: Modeling, applications and biological interpretations. *J. Theor. Biol.* **2006**, *238*, 841–862. https://doi.org/10.1016/j.jtbi.2005.06.037.
6. Eftimie, R.; Bramson, J.L.; Earn, D.J.D. Interactions between the immune system and cancer: A brief review of non-spatial mathematical models. *Bull. Math. Biol.* **2011**, *73*, 2–32.
7. Castiglione, F.; Piccoli, B. Optimal control in a model of dendritic cell transfection cancer immunotherapy. *Bull. Math. Biol.* **2006**, *68*, 255–274. https://doi.org/10.1007/s11538-005-9014-3.
8. Castiglione, F.; Piccoli, B. Cancer immunotherapy, mathematical modeling and optimal control. *J. Theor. Biol.* **2007**, *247*, 723–732.
9. Piccoli, B.; Castiglione, F. Optimal vaccine scheduling in cancer immunotherapy. *Physica A* **2006**, *370*, 672–680.
10. de Pillis, L.G.; Gallegos, A.; Radunskaya, A.E. A model of dendritic cell therapy for melanoma. *Front. Oncol.* **2013**, *3*, 56. https://doi.org/10.3389/fonc.2013.00056.
11. Kamran, M.; Abdullah, J.Y.; Majeed, A. Mathematical modeling for tumor–immune dynamics with clinical validation. *Math. Comput. Appl.* **2026**, *31*, 123. https://doi.org/10.3390/mca31040123.
12. Bonfanti, A.; Kaplan, J.L.; Charras, G.; Kabla, A. Fractional viscoelastic models for power-law materials. *Soft Matter* **2020**, *16*, 6002–6020. https://doi.org/10.1039/d0sm00354a.
13. Bolton, L.; Cloot, A.H.J.J.; Schoombie, S.W.; Slabbert, J.P. A proposed fractional-order Gompertz model and its application to tumour growth data. *Math. Med. Biol.* **2015**, *32*, 187–207.
14. Kumar, D.; Seadawy, A.R.; Joardar, A.K. Modified Kudryashov method via new exact solutions for some conformable fractional differential equations arising in mathematical biology. *Chin. J. Phys.* **2018**, *56*, 75–85. https://doi.org/10.1016/j.cjph.2017.11.020.
15. Wang, X.; Wang, H. Contemporary delay differential equation models and analysis in mathematical biology. In *Contemporary Research in Mathematical Biology—Modeling, Computation and Analysis*; World Scientific: Singapore, 2022.
16. Ghanbari, B. A fractional system of delay differential equations with nonsingular kernels in modeling hand-foot-mouth disease. *Adv. Differ. Equ.* **2020**, *2020*, 536. https://doi.org/10.1186/s13662-020-02993-3.
17. Caputo, M. Linear models of dissipation whose *Q* is almost frequency independent—II. *Geophys. J. R. Astron. Soc.* **1967**, *13*, 529–539.
18. Kilbas, A.A.; Srivastava, H.M.; Trujillo, J.J. *Theory and Applications of Fractional Differential Equations*; Elsevier: Amsterdam, The Netherlands, 2006.
19. Diethelm, K. *The Analysis of Fractional Differential Equations*; Springer: Berlin, Germany, 2010.
20. Odibat, Z.M.; Shawagfeh, N.T. Generalized Taylor's formula. *Appl. Math. Comput.* **2007**, *186*, 286–293.
21. Ouyang, Z. Existence and uniqueness of the solutions for a class of nonlinear fractional-order partial differential equations with delay. *Comput. Math. Appl.* **2011**, *61*, 860–870. https://doi.org/10.1016/j.camwa.2010.12.034.
22. Li, Y.; Chen, Y.; Podlubny, I. Stability of fractional-order nonlinear dynamic systems: Lyapunov direct method and generalized Mittag–Leffler stability. *Comput. Math. Appl.* **2010**, *59*, 1810–1821. https://doi.org/10.1016/j.camwa.2009.08.019.
23. Vargas-De-León, C. Volterra-type Lyapunov functions for fractional-order epidemic systems. *Commun. Nonlinear Sci. Numer. Simul.* **2015**, *24*, 75–85. https://doi.org/10.1016/j.cnsns.2014.12.013.
24. Öztürk, İ.; Özköse, F. Stability analysis of fractional order mathematical model of tumor–immune system interaction. *Chaos Solitons Fractals* **2020**, *133*, 109614. https://doi.org/10.1016/j.chaos.2020.109614.

25. Rihan, F.A.; Velmurugan, G. Dynamics of fractional-order delay differential model for tumor–immune system. *Chaos Solitons Fractals* **2020**, *132*, 109592.
26. Rihan, F.A.; Udhayakumar, K. Fractional order delay differential model of a tumor–immune system with vaccine efficacy: Stability, bifurcation and control. *Chaos Solitons Fractals* **2023**, *173*, 113670.
27. Balçı, E.; Öztürk, İ.; Kartal, S. Dynamical behaviour of fractional order tumor model with Caputo and conformable fractional derivative. *Chaos Solitons Fractals* **2019**, *123*, 43–51. https://doi.org/10.1016/j.chaos.2019.03.032.
28. Uçar, E.; Özdemir, N. A fractional model of cancer–immune system with Caputo and Caputo–Fabrizio derivatives. *Eur. Phys. J. Plus* **2021**, *136*, 43. https://doi.org/10.1140/epjp/s13360-020-00966-9.
29. Ghanbari, B. On the modeling of the interaction between tumor growth and the immune system using some new fractional and fractional-fractal operators. *Adv. Differ. Equ.* **2020**, *2020*, 585.
30. Özköse, F.; Yılmaz, S.; Yavuz, M.; Öztürk, İ.; Şenel, M.T.; Bağcı, B.Ş.; Doğan, M.; Önal, Ö. A fractional modeling of tumor–immune system interaction related to lung cancer with real data. *Eur. Phys. J. Plus* **2022**, *137*, 40.
31. Kumar, S.; Kumar, A.; Samet, B.; Gómez-Aguilar, J.F.; Osman, M.S. A chaos study of tumor and effector cells in fractional tumor–immune model for cancer treatment. *Chaos Solitons Fractals* **2020**, *141*, 110321.
32. Nuruddeen, R.I. Analytical solution for time-fractional diffusion equation by Aboodh decomposition method. *J. King Saud Univ. Sci.* **2017**, *29*, 52–57.
33. Merdan, M.; Şahin, Y.; Açıkgöz, P. The novel numerical solutions for the Caputo–Fabrizio fractional Newell–Whitehead–Segel equation by using Aboodh–ADM. *Res. Sq.* **2024**, *Preprint*. https://doi.org/10.21203/rs.3.rs-4287125/v1.
34. Al-Aati, A.; Al-Sharai, W.M. Exact solution of linear and nonlinear system of partial differential equations by double Aboodh–Shehu and Adomian decomposition method. *Albaydha Univ. J.* **2023**, *5*, 332–346. https://doi.org/10.56807/buj.v5i5.534.
35. Noor, S.; Albalawi, W.; Shah, R.; Shafee, A.; Ismaeel, S.M.E.; El-Tantawy, S.A. A comparative analytical investigation for some linear and nonlinear time-fractional partial differential equations in the framework of the Aboodh transformation. *Front. Phys.* **2024**, *12*, 1374049. https://doi.org/10.3389/fphy.2024.1374049.
36. Shah, R.; Khan, H.; Kumam, P.; Arif, M.; Baleanu, D. Natural transform decomposition method for solving fractional-order partial differential equations with proportional delay. *Mathematics* **2019**, *7*, 532. https://doi.org/10.3390/math7060532.
37. Bekela, A.S.; Belachew, M.T.; Wole, G.A. A numerical method using Laplace-like transform and variational theory for solving time-fractional nonlinear partial differential equations with proportional delay. *Adv. Differ. Equ.* **2020**, *2020*, 586. https://doi.org/10.1186/s13662-020-03048-3.
38. Bekela, A.S.; Woldaregay, M.M. Natural transform method with modified ADM for nonlinear time-fractional PDEs with proportional delay. *Res. Sq.* **2025**, *Preprint*. https://doi.org/10.21203/rs.3.rs-7741477/v1.
39. Alsulami, M.; Al-Mazmumy, M.; Al-Yazidi, N.S. Effective iterative procedure for delay fractional partial differential equations using Sumudu decomposition method. *Symmetry* **2026**, *18*, 407. https://doi.org/10.3390/sym18030407.
40. Sedeeg, A.K.; Mahamoud, Z.I.; Saadeh, R. Using double integral transform (Laplace–ARA transform) in solving partial differential equations. *Symmetry* **2022**, *14*, 2418. https://doi.org/10.3390/sym14112418.
41. Prakasha, D.G.; Veeresha, P.; Baskonus, H.M. Residual power series method for fractional Swift–Hohenberg equation. *Fractal Fract.* **2019**, *3*, 9. https://doi.org/10.3390/fractalfract3010009.
42. Singh, B.K.; Kumar, P. Homotopy perturbation transform method for solving fractional partial differential equations with proportional delay. *SeMA J.* **2018**, *75*, 111–125. https://doi.org/10.1007/s40324-017-0117-1.
43. Dogan, D.D.; Konuralp, A. Fractional variational iteration method for time-fractional nonlinear functional partial differential equation having proportional delays. *Therm. Sci.* **2018**, *22*, S33–S46.
44. Farhood, A.K.; Mohammed, O.H. Homotopy perturbation method for solving time-fractional nonlinear variable-order delay partial differential equations. *Partial Differ. Equ. Appl. Math.* **2023**, *7*, 100513. https://doi.org/10.1016/j.padiff.2023.100513.
45. Yang, X.J. A new integral transform method for solving steady heat-transfer problem. *Therm. Sci.* **2016**, *20*, S639–S642. https://doi.org/10.2298/TSCI16S3639Y.
46. Ganie, A.H.; AlBaidani, M.M.; Khan, A. A comparative study of the fractional partial differential equations via novel transform. *Symmetry* **2023**, *15*, 1101. https://doi.org/10.3390/sym15051101.
47. Ganie, A.H.; Mofarreh, F.; Khan, A. A novel analysis of the time-fractional nonlinear dispersive $K(m,n,1)$ equations using the homotopy perturbation transform method and Yang transform decomposition method. *AIMS Math.* **2024**, *9*, 1877–1898.
48. Abdali, M.H. An iterative approach for solving fractional differential equations using YJ Adomian decomposition method. *Int. J. Appl. Math.* **2025**, *38*, 1244–1256. https://doi.org/10.12732/ijam.v38i2s.717.
49. Al-Griffi, T.A.J.; Al-Saif, A.-S.J. Yang transform–homotopy perturbation method for solving a non-Newtonian viscoelastic fluid flow on the turbine disk. *Z. Angew. Math. Mech.* **2022**, *102*, e202100116. https://doi.org/10.1002/zamm.202100116.
50. Naeem, M.; Yasmin, H.; Shah, R.; Shah, N.A.; Chung, J.D. A comparative study of fractional partial differential equations with the help of Yang transform. *Symmetry* **2023**, *15*, 146. https://doi.org/10.3390/sym15010146.

51. Ganie, A.H.; Khan, A.; Alharthi, N.S.; Tolasa, F.T.; Jeelani, M.B. Comparative analysis of time-fractional coupled system of shallow-water equations including Caputo's fractional derivative. *J. Math.* **2024**, *2024*, 2440359. https://doi.org/10.1155/jom/2440359.
52. Ali, M.A.; Merdan, M. Solution of time-fractional coupled Burgers equations by the Yang transform Adomian decomposition method. *J. Appl. Math.* **2026**, *2026*, 1388808. https://doi.org/10.1155/jama/1388808.
53. Ali, M.A.; Merdan, M. Approximate analytical solutions of the time-fractional Swift–Hohenberg equation via Yang transform Adomian decomposition method. *J. Appl. Math.* **2026**, *2026*, 5815304. https://doi.org/10.1155/jama/5815304.
54. Abubaker, A.A.; Matarneh, K.; Al-Shaikh, S.B.; Khan, M.F. Some new applications of the fractional integral and four-parameter Mittag-Leffler function. *PLoS ONE* **2025**, *20*, e0317776. https://doi.org/10.1371/journal.pone.0317776
55. Mainardi, F. Why the Mittag-Leffler function can be considered the Queen function of the Fractional Calculus? *Entropy* **2020**, *22*, 1359. https://doi.org/10.3390/e22121359.
56. van den Driessche, P.; Watmough, J. Reproduction numbers and sub-threshold endemic equilibria for compartmental models of disease transmission. *Math. Biosci.* **2002**, *180*, 29–48. https://doi.org/10.1016/S0025-5564(02)00108-6.

Disclaimer/Publisher's Note: The statements, opinions and data contained in all publications are solely those of the individual author(s) and contributor(s) and not of MDPI and/or the editor(s). MDPI and/or the editor(s) disclaim responsibility for any injury to people or property resulting from any ideas, methods, instructions or products referred to in the content.